NACA

RESEARCH MEMORANDUM

AERODYNAMIC CHARACTERISTICS OF A 45° SWEPTBACK WING-FUSELAGE COMBINATION AND THE FUSELAGE ALONE OBTAINED IN THE LANGLEY 8-FOOT TRANSONIC TUNNEL

By Robert S. Osborne and John P. Mugler, Jr.

Langley Aeronautical Laboratory
Langley Field, Va.

NATIONAL ADVISORY COMMITTEE
FOR AERONAUTICS

WASHINGTON

September 16, 1952

NATIONAL ADVISORY COMMITTEE FOR AERONAUTICS

RESEARCH MEMORANDUM

AERODYNAMIC CHARACTERISTICS OF A 45° SWEPTBACK WING-FUSELAGE COMBINATION AND THE FUSELAGE ALONE OBTAINED IN THE LANGLEY 8-FOOT TRANSONIC TUNNEL

By Robert S. Osborne and John P. Mugler, Jr.

SUMMARY

A fuselage and a wing-fuselage combination employing a wing with 45° sweepback of the 0.25-chord line, aspect ratio 4, taper ratio 0.6, and NACA 65A006 airfoil sections have been investigated in the slotted test section of the Langley 8-foot transonic tunnel at Mach numbers from 0.6 to 1.13 for angles of attack up to 36°. Maximum lift was reached at Mach numbers from 0.6 to 0.92.

For the wing-fuselage configuration increases in Mach number at low lift coefficients resulted in an increase in lift-curve slope up to a Mach number of 0.91, a rapid increase in drag between the Mach numbers of 0.93 and 1.04, rearward shifts of the aerodynamic center up to a Mach number of 1.0, and a reduction in maximum lift-drag ratio from 14 at subcritical speeds to 7.5 at Mach numbers above 1.03. With increases in lift coefficient from 0.3 to 0.6 the growth of leading-edge separation increased the lift-curve slope, decreased leading-edge suction, and shifted the aerodynamic center rearward. At lift coefficients above 0.6 more extensive flow separation caused decreases in the lift-curve slope and large very abrupt forward and rearward movements of the aerodynamic center.

INTRODUCTION

As part of a general National Advisory Committee for Aeronautics research program the aerodynamic characteristics of a fuselage and a wing-fuselage configuration employing a wing with 45° sweepback of the 0.25-chord line, an aspect ratio of 4, a taper ratio of 0.6, and NACA 65A006 airfoil sections parallel to the plane of symmetry have

been investigated at transonic speeds by the transonic-bump, rocket, and free-fall techniques. The results are reported in references 1, 2, 3, and 4.

In addition, force tests of sting-supported models of these configurations were conducted at angles of attack up to 14° at Mach numbers from 0.6 to 0.96 and at a Mach number of 1.2 in the Langley 8-foot high-speed tunnel. The results are presented in reference 5. Subsequently a slotted nozzle was installed in the tunnel (ref. 6), and a comparatively complete investigation of the configurations, including force and pressure-distribution tests and flow surveys, was conducted at Mach numbers varying continuously from 0.6 to 1.13. The results of the pressure-distribution tests are reported in reference 7. The loading characteristics obtained are discussed in references 8 and 9 and the flow phenomena in reference 10.

There is relatively little information available on the characteristics of fuselage and wing-fuselage configurations at high angles of attack in the transonic Mach number range, and therefore, in appreciation of the need of aircraft and missile designers for more of these data, the angle-of-attack range of the force tests of these configurations in the slotted tunnel was extended to 36°. Lift, drag, pitching-moment, and base pressure coefficients were obtained, and some boundary-layer characteristics were determined from tuft surveys. The results are presented in this paper.

SYMBOLS

A aspect ratio

C_D drag coefficient, D/qS

C_{D_o} drag coefficient at zero lift

ΔC_D = Interference-free drag coefficient - Measured drag coefficient

C_L lift coefficient, L/qS

$\frac{\partial C_L}{\partial \alpha}$ lift-curve slope per degree

C_m pitching-moment coefficient, $\frac{M_{\bar{c}/4}}{qS\bar{c}}$

[redacted]

$\frac{\partial C_m}{\partial C_L}$	static-longitudinal-stability parameter
$\bar{c}$	wing mean aerodynamic chord, in.
D	drag, lb
L	lift, lb
M	average stream Mach number
$M_{\bar{c}/4}$	pitching moment about $0.25\bar{c}$, in.-lb
P_b	base pressure coefficient, $\frac{p_b - p_o}{q}$
ΔP_b	incremental base pressure coefficient due to addition of wing to fuselage
p_o	free-stream static pressure, lb/sq ft
p_b	static pressure at model base, lb/sq ft
q	free-stream dynamic pressure, $\frac{1}{2}\rho V^2$, lb/sq ft
R	Reynolds number based on $\bar{c}$
S	wing area, sq ft
V	free-stream velocity, ft/sec
α	angle of attack of fuselage center line, deg
θ_t	angle of wing-tip twist, deg, Angle of attack of wing-tip chord - α
ρ	free-stream density, slugs/cu ft

APPARATUS AND METHODS

Tunnel

The tests were conducted in the Langley 8-foot transonic tunnel which is a dodecagonal slotted-throat, single-return wind tunnel designed to obtain aerodynamic data through the speed of sound without the usual effects of choking and blockage. The tunnel operates at atmospheric stagnation pressures.

As was shown in reference 11, the flow in the region of the test section occupied by the model was satisfactorily uniform at all test Mach numbers. Local deviations from the average stream Mach number were no larger than 0.003 at subsonic speeds. With increases in Mach number above 1.0, the deviations increased but did not exceed 0.010 at a Mach number of 1.13. Tests reported in reference 12 indicated that local flow nonuniformities of this magnitude had no effect on the measured force data. Some typical Mach number distributions and the relative axial positions of the slots, test region, and approximate model location are shown in figure 1.

Model

A photograph of the wing-fuselage configuration is presented as figure 2 and dimensional details are shown in figure 3 and table I. The wing had 45° sweepback of the 0.25-chord line, an aspect ratio of 4, a taper ratio of 0.6, and NACA 65A006 airfoil sections parallel to the model plane of symmetry and was of solid steel construction.

The first part of the investigation consisted of tests of a fuselage of hollow steel construction designed by cutting off the rear portion of a basic body of revolution with a fineness ratio of 12 to form a body with a fineness ratio of 10. The body with a fineness ratio of 10 is referred to hereinafter as the original fuselage. After completion of these tests the internal strain-gage balance failed and a balance of slightly larger diameter was substituted. The rear portions of the original fuselage, however, fouled the larger balance at comparatively low loads and the subsequent enlargement of the interior of the body necessitated removal of approximately 2 percent of the aft end. The shorter body had a fineness ratio of 9.8 and is referred to herein as the fuselage. Details of the fuselages are presented in figure 4 and table I. The ratio of wing area to fuselage frontal area was 16.5.

The wing was tested on the fuselage at an angle of incidence of 0°. Vertically it was located at the horizontal diameter of the fuselage and was rigidly attached at the wing-fuselage juncture.

[redacted]

Model Support System

The model was attached to an enclosed strain-gage balance at its forward end. At its downstream end the balance was attached to a support tube through couplings which were varied to keep the model close to the center line of the tunnel at all angles of attack. The support tube was fixed axially in the center of the tunnel by two sets of support struts projecting from the tunnel walls. A typical support configuration is shown in figure 5.

Details of the mechanism for changing angle of attack with the tunnel operating are presented in reference 5.

Measurements and Accuracy

The average stream Mach number was determined to within ±0.003 from a calibration with respect to the pressure in the chamber surrounding the slotted test section.

Lift, drag, and pitching moment were determined by means of a strain-gage balance located inside the fuselage. The measured coefficients were estimated to be accurate within the following limits:

	C_L	C_D	C_m
Original fuselage	±0.01	±0.001	±0.005
Fuselage	±0.02	±0.002	±0.004
Wing-fuselage	±0.02	±0.002	±0.004

The base pressure was determined from a static orifice located on the side of the sting support in the plane of the model base. The base pressure coefficient was estimated to be accurate within ±0.003.

The angle of attack of the model was measured by an optical cathetometer sighted on a reference line on the side of the fuselage. A consideration of the accuracy of the cathetometer readings (±0.1°) and the flow angularity measurements (±0.1°) indicated that the angle of attack was accurate to within ±0.2°. The angles of wing-tip twist were determined from measurements of the angles of attack of the wing-tip chord obtained by sighting the cathetometer on a reference line at the tip. Due to vibration of the tip and the relatively short reference line, the angles of wing-tip twist may be in error as much as ±0.3°.

Test Conditions

The tests were conducted through a Mach number range from 0.6 to approximately 1.13. The Reynolds number based on the wing mean aerodynamic chord was of the order of 2×10^6 (fig. 6). The wing-fuselage

configuration was tested at angles of attack from 0° to 36°. Above 20° angle of attack, however, load limitations of the balance prevented testing at some of the higher Mach numbers. The fuselage configurations were tested at angles of attack from -4° to 36°.

A tuft survey was conducted on the wing-fuselage configuration at angles of attack from -4° to 20°. Alternate rows of woolen yarn and nylon tufts were glued on the upper surface of the left wing and on the upper left half of the fuselage. The tuft patterns were photographed at several Mach numbers at each angle of attack.

CORRECTIONS

Boundary Interference

Subsonic speeds.- The axially slotted test section minimized boundary interference due to solid blockage (ref. 13), and a qualitative analysis indicated that other subsonic boundary interference effects on the data presented herein were either negligible or very small up to the highest angles of attack tested. Experimental evidence of these small effects is indicated in figure 7, which presents a comparison of some representative data for the wing-fuselage configuration with data obtained from tests of the same model and strain-gage balance in the Langley 16-foot transonic tunnel. The comparatively large cross-sectional area and axially slotted boundary of the test section of the latter facility insured that data obtained for the relatively small model at subsonic speeds were interference-free. The only appreciable disagreement between the two sets of data at Mach numbers below 1.0 occurred in drag coefficient at an angle of attack of 32°. It is notable, however, that the difference in magnitude was less than 2 percent of the total drag coefficient and, when considered in conjunction with the difference in lift coefficient, appeared to have been due to a discrepancy in angle of attack which was less than the sum of the probable errors in angle-of-attack measurement for the two tests.

Supersonic speeds.- Boundary interference effects at Mach numbers above 1.0 consisted of shocks and expansions from the model which were reflected back to the surface of the model by the test-section boundary. For the present case, these disturbances passed downstream of the model base at a Mach number of approximately 1.1 and data for all higher Mach numbers were completely free of interference.

However, even in the Mach number range where boundary-reflected disturbances reached the model, the effects on the force and moment characteristics of the present configurations were small. These effects

are evident from the comparisons presented in figure 7. The Langley 16-foot transonic-tunnel data for these models were shown in reference 11 to be free of boundary-reflected disturbances except at a Mach number of approximately 1.015 and therefore provided a basis for evaluating these effects on the present data. The indication was that the effects were negligible for lift coefficient, increased the drag coefficient at low angles of attack as much as 0.002 at a Mach number of approximately 1.04, decreased it as much as 0.002 at a Mach number of approximately 1.09, and decreased the pitching-moment coefficient on the order of 0.005 at high angles of attack at a Mach number of approximately 1.06. These errors have been minimized by fairing the data plotted against Mach number, and it is believed that none of the general trends exhibited by the faired data or the conclusions drawn therefrom were affected by boundary-reflected disturbances.

It must be emphasized that the effects of boundary-reflected disturbances discussed apply only to the specific models described herein. Configurations employing a horizontal tail and bodies of different shape and length, for example, might be expected to sustain considerably different effects than did the present models.

Aeroelasticity

No corrections for the effects of wing elasticity have been applied to the data presented herein. Comparisons with unpublished data obtained for angles of attack up to 20° on an identical configuration employing a relatively flexible wing constructed of aluminum alloy indicated that aeroelastic effects on the lift and drag of the present steel wing were negligible and that the aerodynamic center was moved forward approximately 1 percent of the mean aerodynamic chord as compared with a rigid wing. The measured angles of wing-tip twist shown in figure 8 were small and were indicative of the rigidity of the steel wing.

Sting Interference

Sting interference probably had no effect on the lift and pitching moment of the models (ref. 14). Decreases in drag coefficient due to sting interference were estimated as outlined in reference 5 and are presented in figure 9. These estimates were based on the assumption that the present bodies were identical to the body of reference 14. Values for the fuselage also apply to the wing-fuselage configuration. Because of the uncertainty of these values, especially at high angles of attack, no corrections have been applied to data presented herein except in plots of drag at zero lift and in calculations of lift-drag ratio.

The presence of the sting was estimated to increase the base pressure coefficients on the order of 0.1 at all Mach numbers tested for low angles of attack (ref. 5). No corrections have been applied, however, to the base pressure coefficients presented herein.

RESULTS

An index of figures 10 to 31 presenting the results is shown in table II.

For lift coefficients up to approximately 0.8 improved accuracy of the force and moment characteristics of the wing-fuselage configuration at constant Mach number (fig. 12) has been obtained, despite the relatively large increments between test points, by fairing the data in accordance with unpublished data obtained from a model differing from the present one only in wing stiffness which was tested at angle-of-attack increments of 2° or less.

In the intervals of angle of attack where test points for the fuselage were not available, these data were faired to conform to the more complete original fuselage data (fig. 13) and interpolated values for the fuselage were subtracted from the wing-fuselage data to obtain the force and moment coefficients for the wing with wing-fuselage interference (fig. 14). It can be assumed that these wing-plus-interference data require no corrections for sting interference.

Since the model was symmetrical about the wing-chord plane, the tuft patterns over the upper surface at an angle of attack of -4° (fig. 28) also apply to the lower surface at an angle of attack of 4°.

The base-pressure coefficients for the fuselage (fig. 30) were subtracted from those for the wing-fuselage configuration (fig. 29) to obtain the incremental values due to addition of the wing to the fuselage which are presented in figure 31. These increments were probably unaffected by sting interference.

In order to facilitate presentation of the data, staggered scales have been used in many of the figures and care should be taken in selecting the zero axis for each curve.

DISCUSSION

The force and moment characteristics were probably not significantly altered by the comparatively low test Reynolds number. It was indicated

in reference 15 and by unpublished results of tests of similar wings at high subsonic Mach numbers that scale effects were small as the Reynolds number was varied from 1.2×10^6 to at least 8.5×10^6.

Discussion concerning pressure distributions and wing loading is based on pressure measurements obtained on a similar configuration and reported in reference 7. The force data at a Mach number of 1.2 were obtained from reference 5 and have been corrected for differences in wing elasticity.

Lift Characteristics

Wing-fuselage configuration.- The effects of increasing Mach number at constant angle of attack for the wing-fuselage configuration at angles of attack up to 10° consisted of a gradual increase in lift coefficient up to a Mach number of 0.92, followed by a small decrease up to the highest test Mach number (fig. 10(a)). At high angles of attack the characteristic effect was a rapid increase in lift coefficient beginning at Mach numbers varying from 0.92 at an angle of attack of 12° to 0.84 at an angle of attack of 36° and ending at a Mach number of approximately 1.01. The rapid increase in lift with increasing Mach number at an angle of attack of 12° was due to an increase in loading over the outboard forward portions of the wing, while at an angle of attack of 20° it was due to an increase in loading over the entire wing. Increases in Mach number from 1.01 to 1.11 resulted in reductions in lift coefficient of approximately 5 percent.

The lift-curve slope at zero lift (fig. 15) increased approximately 29 percent from 0.059 at a Mach number of 0.6 to 0.076 at a Mach number of 0.91. With further increases in Mach number the lift-curve slope decreased to a value of 0.067 at a Mach number of 1.13 and 0.062 at a Mach number of 1.2. At a lift coefficient of 0.4 ($\alpha \approx 6°$) similar trends with Mach number were indicated, with the lift-curve slopes being approximately 13 percent greater at Mach numbers from 0.6 to 0.85 and 5 percent greater at higher Mach numbers. This increase was probably due to a leading-edge separation vortex such as that described in reference 16. The leading-edge separation was indicated in the pressure distributions by leading-edge negative pressure peaks which became progressively lower and broader from the wing root to the tip and was shown in the tuft patterns by an outward redirection of the boundary layer along the leading edge (figs. 28(a) and 28(b), $\alpha = 6°$ and 8°). A comparison of figures 28(a) and 28(c) showed that the outward flow had been eliminated along the leading edge of the inboard portion of the semispan at Mach numbers of 0.84 and above and indicated that the separation vortex was no longer present in those regions.

With increases in lift coefficient above 0.6 ($\alpha \approx 8^\circ$) extensive and severe flow separation beginning at the wing tips, shown by the turning outward and rapid fluctuation of the tufts (fig. 28), caused the lift-curve slopes of the wing-fuselage configuration to decrease (fig. 12(a)). Because of a general rearward and outboard contraction of the area of separated flow with increases in Mach number above 0.89 (compare fig. 28(d) with fig. 28(i), $\alpha = 10^\circ$ and 12°), the losses in lift-curve slope were more severe at the lower Mach numbers. For example, at Mach numbers from 0.6 to 0.84, it was indicated that maximum lift was being approached at an angle of attack of 18°. However, further increases in angle of attack resulted in substantial increases in lift-curve slope until the angle of attack for maximum lift was approached. The maximum lift coefficients increased from 1.01 to 1.15 at Mach numbers from 0.6 to 0.92 (fig. 16(a)) and occurred at angles of attack from 31° to 33° (fig. 16(b)). Maximum lift was not attained in this investigation at Mach numbers above 0.92 because of fouling between the model and the strain-gage balance.

Fuselage.- At constant angle of attack the lift coefficients for the fuselages (fig. 11(a)) did not vary with Mach number up to an angle of attack of 20°. At higher angles a small, approximately linear increase in lift coefficient with Mach number was indicated. The lift-curve slopes generally increased slightly with increasing angle of attack (fig. 13(a)) and, at angles of attack above 20°, they also increased with Mach number.

Drag Characteristics

Wing-fuselage configuration.- The variations of drag coefficient with Mach number at constant angle of attack for the wing-fuselage configuration (fig. 10(b)) indicated a drag increase of approximately 0.013 between the Mach numbers of 0.93 and 1.04 at an angle of attack of 0°. The magnitude of the drag rise and the Mach number range over which it occurred increased as the angle of attack was increased to 36°. The appreciable decrease in drag coefficient which began at a Mach number of approximately 1.01 at angles of attack above 8°, combined with the reduction in lift coefficient previously discussed, resulted in drag polars of constant shape in this region (see fig. 12(b)). It must be noted again that the basic drag data presented in figures 10 to 13 include the effects of sting interference and that this accounts for the apparently low values of drag coefficient for the wing-fuselage and fuselage configurations at an angle of attack of 0°.

The drag coefficients at zero lift for the wing-fuselage configuration were corrected for sting interference (representing support-free, power-off conditions) and are shown in figure 17. An increase in drag

[redacted]

coefficient of approximately 120 percent occurred between the Mach numbers of 0.93 and 1.04. Since the tuft patterns for an angle of attack of 0° (fig. 28) were not indicative of boundary-layer separation, most of this drag rise must have been due to shock losses alone rather than to shock-induced separation.

The variations of drag coefficient due to lift with lift coefficient squared for lift coefficients up to approximately 0.6 are shown for several Mach numbers in figure 18 along with the ideal induced drag $C_L^2/\pi A$ and the theoretical drag due to lift with no leading-edge suction $C_L \tan \alpha$. At a Mach number of 0.6 leading-edge suction reduced the drag due to lift approximately 50 percent for lift coefficients up to 0.3. At higher lift coefficients, however, the leading-edge suction was decreased by the onset of the leading-edge separation previously discussed. With increases in Mach number the effects of leading-edge suction were apparently reduced at all lift coefficients. At a lift coefficient of 0.55, for example, the drag due to lift with no leading-edge suction was decreased 21 percent at a Mach number of 0.6, 15 percent at a Mach number of 0.89, and only 11 percent at Mach numbers of 0.99 and above. It should be noted that the wing leading edges were swept behind the Mach line at all Mach numbers tested and that the apparent loss in leading-edge suction at high Mach numbers was due to the development of supersonic-type flow over the leading edges and to increased drag resulting from separation near the trailing edges of the wing.

The variations of drag coefficient with lift coefficient squared for lift coefficients up to approximately 1.0 (fig. 19) indicated drag increases at lift coefficients above 0.6 which resulted in large departures from the straight line indicative of a parabolic drag polar. The very large drag increases at the lower Mach numbers were substantially alleviated at Mach numbers above 0.89 as a result of contraction of the regions of separated flow.

Fuselage.- At constant angle of attack the drag rises for the fuselage configurations increased in magnitude and began at lower Mach numbers as the angle of attack was varied from 0° to 36° (fig. 11(b)). The drag coefficients at zero lift for the original fuselage, which are presented corrected for sting interference in figure 17, increased 80 percent between the Mach numbers of 0.99 and 1.04. This drag rise was probably due almost entirely to the formation of strong shocks on the aft portions of the body. No separation was evident in the tuft patterns in figure 28. The mechanism of the drag rise for a similar body is discussed in some detail in reference 3.

The drag peak occurring at a Mach number of 1.01 for the wing with wing-fuselage interference (fig. 17) was probably the result of

wing-fuselage interference which reduced the pressures over the rearward portions and the base of the fuselage (see fig. 31).

Lift-Drag Ratios

Wing-fuselage configuration.- The lift-drag ratios for the wing-fuselage configuration (fig. 20) have been corrected for the effects of sting interference on drag and therefore represent the configuration in a support-free, power-off condition. The values of maximum lift-drag ratio (fig. 21) decreased from 14 at subcritical Mach numbers to approximately 7.5 at Mach numbers above 1.03. The rapid decrease beginning at a Mach number of approximately 0.91 was caused primarily by the drag rise previously discussed. The lift coefficient for maximum lift-drag ratio (fig. 22) increased from 0.23 at Mach numbers up to 0.91 to 0.33 for Mach numbers above 1.1.

Pitching-Moment Characteristics

Wing-fuselage configuration.- For lifting conditions, increases in Mach number up to approximately 1.01 for the wing-fuselage configuration at constant angle of attack resulted in decreases in pitching-moment coefficient (fig. 10(c)) which became more severe as the angle of attack was increased. For angles of attack up to approximately 12° the reductions in pitching-moment coefficient with increasing Mach number were due largely to a rearward shift in the chordwise center of pressure associated with an outboard shift in spanwise loading; whereas at higher angles of attack they were caused primarily by rapidly increasing lift in combination with smaller rearward shifts in the center of pressure (see fig. 10(a)). The variations of pitching-moment coefficient with Mach number were small at Mach numbers above 1.01 except for an angle of attack of 12°, where pressure distributions indicated a continuing rearward and outward movement of the center of pressure.

The variations of static-longitudinal-stability parameter $\partial C_m/\partial C_L$ with Mach number (fig. 23) indicated that at zero lift the aerodynamic center was 5 percent of the mean aerodynamic chord ahead of the $\bar{c}/4$ location at a Mach number of 0.6. With increases in Mach number it moved rearward until at a Mach number of 1.00 it was located approximately 19 percent of the mean aerodynamic chord behind the $\bar{c}/4$. The particularly rapid rearward movement between the Mach numbers of 0.91 and 1.00 was caused by substantial rearward and outward shifts in center of pressure. At Mach numbers from 1.00 to 1.2 the aerodynamic-center location remained essentially constant. At a lift coefficient of 0.4 ($\alpha \approx 6°$) the variations of $\partial C_m/\partial C_L$ with Mach number were similar to those at zero lift,

but it was indicated that the aerodynamic center had moved rearward by 8 percent of the mean aerodynamic chord at the lower Mach numbers and 4 percent at Mach numbers above 0.9 as compared with the zero-lift condition. This rearward shift can be attributed to the previously discussed leading-edge separation.

The variations of pitching-moment coefficient with lift coefficient (fig. 12(c)) indicated that at a Mach number of 0.6 increases in lift coefficient above 0.54 ($\alpha = 8^\circ$) resulted in an abrupt forward movement of the aerodynamic center which then remained ahead of the $\bar{c}/4$ up to a lift coefficient of 0.83 ($\alpha = 16^\circ$). With further increases the aerodynamic center moved immediately rearward of the $\bar{c}/4$, and this stabilizing tendency continued up to maximum lift ($\alpha \approx 31^\circ$). At angles of attack beyond maximum lift the pitching-moment effects were destabilizing. Pressure distributions and the tuft patterns shown in figure 28 indicated that the forward movement of the aerodynamic center beginning at an angle of attack slightly above 8° was due to the inboard spreading of strong flow separation over the outboard portions of the wing with an attendant inboard and forward shift of the center of pressure. At an angle of attack of 20° complete separation over the wing resulting in increased loading over the trailing edges of the inboard portions of the semispan caused a rearward movement of the center of pressure.

With increases in Mach number above 0.89 the abrupt forward and rearward movements of the aerodynamic center were delayed to higher lift coefficients. At a Mach number of 1.11 the forward shift occurred at a lift coefficient of 0.75 ($\alpha = 11^\circ$), and it was indicated that the rearward shift occurred at a lift coefficient of approximately 1.11 ($\alpha = 21^\circ$). These delays were the result of increased loading over the outboard portions of the wing caused by the rearward and outward contraction of the regions of flow separation with increasing Mach number (fig. 28).

Increasing Mach number also had a significant effect on the magnitude of the forward shift of the aerodynamic center which occurred at moderate lift coefficients (fig. 24). The forward shift was greatly increased at Mach numbers from 0.79 to 0.99 and reached a maximum of 130 percent of the mean aerodynamic chord at a Mach number of 0.92. This was the result of relative changes in total load and chordwise center-of-pressure location which occurred in this Mach number range for angles of attack from 8° to 16°. There was some indication that the shift also increased at Mach numbers above 1.1; however, it may be concluded that efforts to alleviate these adverse pitch-up characteristics, at least for transonic speeds, should be concentrated at Mach numbers from 0.8 to 1.0.

Fuselage.- For the fuselage configurations at constant angle of attack increases in Mach number up to approximately 1.01 at angles of attack up to 16° resulted in slight increases in pitching-moment coefficient which were no larger than 0.01, (fig. 11(c)). At higher angles of attack increases as large as 0.11 occurred over the same Mach number range. The configurations possessed destabilizing pitching-moment characteristics with respect to the $\bar{c}/4$ location at all Mach numbers and angles of attack tested (fig. 13(c)).

At a Mach number of 0.6 the center of pressure for the original fuselage moved rearward from 11 percent of the fuselage length ahead of the nose at an angle of attack of 4° to 39 percent behind the nose at an angle of attack of 36° (fig. 25). This rearward movement was associated mainly with an increase in the positive pressures over the lower surface of the forward portions of the body. With increases in Mach number from 0.6 to 1.11 the center of pressure moved rearward as much as 27 percent of the fuselage length at angles of attack from 4° to 12°. At higher angles of attack, however, Mach number effects were small.

Comparison With Other Test Results

The force and moment characteristics presented herein were in agreement with those reported in reference 5 with allowance made for differences in wing elasticity. Comparisons were also made with similar data obtained from semispan models tested on the transonic bump of the Langley high-speed 7- by 10-foot tunnel (ref. 1), from flight tests of rocket-powered models (ref. 2), and from free-fall tests (refs. 3 and 4). These data represent wing-fuselage and fuselage-alone models of like shape, with the minor exception that the rear one-sixth of the basic body (see table I) had not been cut off in the case of the free-fall models and the fineness ratio was therefore increased from 10 to 12. The drag data for the sting-supported models have been corrected for sting interference. The approximate test Reynolds numbers, based on the wing mean aerodynamic chord, were as follows:

8-foot transonic tunnel	2×10^6
Bump	0.8×10^6
Rocket	6×10^6 to 14×10^6
Free fall	2×10^6 to 12×10^6

Lift and pitching-moment characteristics.- The variations of lift-curve slope and static-longitudinal-stability parameter $\partial C_m/\partial C_L$ with Mach number for the sting-supported and the bump model of the wing-fuselage configuration are compared in figure 26. The bump model employed a steel wing mounted inside the bump 25 percent semispan from

the fuselage center line. The slopes used for the comparisons were averaged over the lift-coefficient range from zero up to the lift coefficient at which obvious departures from linearity occurred.

The variations of lift-curve slope with Mach number for the two models were in good qualitative agreement (fig. 26(a)); however, the values for the bump model were approximately 4 percent greater than those for the sting-supported model. The variations of $\partial C_m/\partial C_L$ with Mach number (fig. 26(b)) were in excellent agreement. The comparisons of lift coefficient with angle of attack and pitching-moment coefficient with lift coefficient (not shown herein) were similar to those presented in reference 1 for the bump model and for the tests of the sting-supported model which were reported in reference 5. They indicated that the decreases in lift-curve slope and the destabilizing pitching-moment break which occurred at a lift coefficient of the order of 0.6 for the sting-supported model occurred at a lift coefficient approximately 0.1 lower and with less abruptness for the bump model.

Drag characteristics.- The variations of drag coefficient at zero lift with Mach number as obtained from the sting-supported, rocket, and free-fall tests are compared in figure 27. Data for the bump models have not been shown since it was concluded in reference 1 that they were unreliable. The data were in good agreement, the comparison between the sting-supported and free-fall configurations being especially remarkable. The slightly decreased rate of drag rise for the sting-supported fuselage (fig. 27(b)) may have been due to overexpansion of the flow over the forward portion of the body caused by boundary-reflected disturbances (see ref. 11).

The reliability of the present data which was indicated by the comparisons with data from the Langley 16-foot transonic tunnel (fig. 7) was further confirmed by the foregoing comparisons with data obtained by the rocket and free-fall techniques. It was also indicated that boundary-reflected disturbances need not invalidate or obscure the over-all force and moment characteristics of models such as those used in the present investigation.

Base-Pressure Characteristics

Wing-fuselage configuration.- With increases in Mach number at constant angle of attack the base pressure coefficients for the wing-fuselage configuration generally decreased rapidly beginning at Mach numbers varying from 1.0 at an angle of attack of 0° to 0.90 at an angle of attack of 36° (fig. 29). It was shown in reference 17 that the abrupt reductions in base pressure were due to corresponding reductions in pressure on the surface of the fuselage just ahead of the base.

The pressure distributions of reference 7 confirmed this conclusion. At an angle of attack of 0°, for example, it was indicated that the pressures over the body from the 90-percent station to the base were abruptly reduced between the Mach numbers of 0.99 and 1.02. Some of the irregularities in base pressure coefficient in the vicinity of a Mach number of 1.08 may have been due to the passage of boundary-reflected expansions and compressions over the model base. With increases in angle of attack at constant Mach number the base pressures decreased rapidly above angles of attack ranging from 20° at a Mach number of 0.6 to 8° at a Mach number of 1.1.

Fuselage.- With increases in Mach number the base pressure coefficients for the fuselages increased up to a Mach number of approximately 1.01 and then abruptly decreased (fig. 30). At constant Mach number the base pressures were generally reduced with increases in angle of attack. The characteristics for the fuselage were similar to those for the original fuselage except that the values of base pressure coefficient at angles of attack from 20° to 36° were decreased on the order of 0.1.

Addition of the wing to the fuselage at angles of attack up to 8° had no effect on the base pressures of the fuselage except at a Mach number of 1.01, where the base pressure coefficients were reduced approximately 0.07 (fig. 31). At angles of attack from 20° to 36° addition of the wing reduced the base pressure coefficients as much as 0.4 at the higher Mach numbers. These effects were probably caused by wing-fuselage interference which decreased the pressures over the fuselage just forward of the base.

CONCLUSIONS

The following may be concluded from an investigation to determine the aerodynamic characteristics of a 45° sweptback wing-fuselage combination and the fuselage alone at transonic speeds:

1. At low lift coefficients increases in Mach number above 0.6 for the wing-fuselage configuration resulted in an increase in lift-curve slope up to a Mach number of 0.91, a 120-percent increase in drag coefficient between the Mach numbers of 0.93 and 1.04, and a rearward movement of the aerodynamic center ending at a Mach number of 1.0. The maximum lift-drag ratio decreased from 14 at subcritical speeds to 7.5 at Mach numbers above 1.03.

2. The growth of leading-edge separation with increases in lift coefficient from 0.3 to 0.6 caused increases in the lift-curve slope, decreases in leading-edge suction, and a rearward shift of the aerodynamic center.

[redacted]

3. In the lift-coefficient range from 0.6 to maximum lift, the spread of strong separation over the outboard portions of the wing resulted in general decreases in lift-curve slope accompanied by large and exceedingly abrupt forward and rearward shifts of the aerodynamic center. Efforts to alleviate the adverse pitch-up characteristics should be concentrated in the Mach number range from 0.8 to 1.0.

4. At Mach numbers from 0.6 to 0.92, maximum lift coefficients from 1.01 to 1.15 were attained at angles of attack from 31° to 33°.

5. The effects of boundary layer separation on the force and moment characteristics generally decreased with increasing Mach number because of the rearward and outward contraction of the separated regions on the wing.

6. At low angles of attack the drag coefficients for the fuselage increased 80 percent between the Mach numbers of 0.99 and 1.04. The fuselage center of pressure generally moved rearward with increases in angle of attack and Mach number.

Langley Aeronautical Laboratory
National Advisory Committee for Aeronautics
Langley Field, Va.

[redacted]

REFERENCES

1. Donlan, Charles J., Meyers, Boyd C., II, and Mattson, Axel T.: A Comparison of the Aerodynamic Characteristics at Transonic Speeds of Four Wing-Fuselage Configurations as Determined From Different Test Techniques. NACA RM L50H02, 1950.

2. Katz, Ellis: Flight Investigation From High Subsonic to Supersonic Speeds To Determine the Zero-Lift Drag of a Transonic Research Vehicle Having Wings of 45° Sweepback, Aspect Ratio 4, Taper Ratio 0.6, and NACA 65A006 Airfoil Sections. NACA RM L9H30, 1949.

3. Thompson, Jim Rogers: Measurements of the Drag and Pressure Distribution on a Body of Revolution Throughout Transition From Subsonic to Supersonic Speeds. NACA RM L9J27, 1950.

4. Kurbjun, Max C., and Thompson, Jim Rogers: Transonic Drag Characteristics and Pressure Distribution on the Body of a Wing-Body Combination Consisting of a Body of Revolution of Fineness Ratio 12 and a Wing Having Sweepback of 45°, Aspect Ratio 4, Taper Ratio 0.6, and NACA 65A006 Airfoil Sections. NACA RM L52B12, 1952.

5. Osborne, Robert S.: A Transonic-Wing Investigation in the Langley 8-Foot High-Speed Tunnel at High Subsonic Mach Numbers and at a Mach Number of 1.2. Wing-Fuselage Configuration Having a Wing of 45° Sweepback, Aspect Ratio 4, Taper Ratio 0.6, and NACA 65A006 Airfoil Section. NACA RM L50H08, 1950.

6. Wright, Ray H., and Ritchie, Virgil S.: Characteristics of a Transonic Test Section With Various Slot Shapes in the Langley 8-Foot High-Speed Tunnel. NACA RM L51H10, 1951.

7. Loving, Donald L., and Williams, Claude V.: Basic Pressure Measurements on a Fuselage and a 45° Sweptback Wing-Fuselage Combination at Transonic Speeds in the Slotted Test Section of the Langley 8-Foot High-Speed Tunnel. NACA RM L51F05, 1951.

8. Loving, Donald L., and Williams, Claude V.: Aerodynamic Loading Characteristics of a Wing-Fuselage Combination Having a Wing of 45° Sweepback Measured in the Langley 8-Foot Transonic Tunnel. NACA RM L52B27, 1952.

9. Estabrooks, Bruce B.: An Analysis of the Pressure Distribution Measured on a Body of Revolution at Transonic Speeds in the Slotted Test Section of the Langley 8-Foot Transonic Tunnel. NACA RM L52D21a, 1952.

[redacted]

10. Whitcomb, Richard T., and Kelly, Thomas C.: A Study of the Flow Over a 45° Sweptback Wing-Fuselage Combination at Transonic Mach Numbers. NACA RM L52D01, 1952.

11. Ritchie, Virgil S., and Pearson, Albin O.: Calibration of the Slotted Test Section of the Langley 8-Foot Transonic Tunnel and Preliminary Experimental Investigation of Boundary-Reflected Disturbances. NACA RM L51K14, 1951.

12. Ritchie, Virgil S.: Effects of Certain Flow Nonuniformities on Lift, Drag, and Pitching Moment for a Transonic-Airplane Model Investigated at a Mach Number of 1.2 in a Nozzle of Circular Cross Section. NACA RM L9E20a, 1949.

13. Wright, Ray H., and Ward, Vernon G.: NACA Transonic Wind-Tunnel Test Sections. NACA RM L8J06, 1948.

14. Osborne, Robert S.: High-Speed Wind-Tunnel Investigation of the Longitudinal Stability and Control Characteristics of a $\frac{1}{16}$-Scale Model of the D-558-2 Research Airplane at High Subsonic Mach Numbers and at a Mach Number of 1.2. NACA RM L9C04, 1949.

15. Lowry, John G., and Cahill, Jones F.: Review of the Maximum-Lift Characteristics of Thin and Swept Wings. NACA RM L51E03, 1951.

16. Cahill, Jones F., and Gottlieb, Stanley M.: Low-Speed Aerodynamic Characteristics of a Series of Swept Wings Having NACA 65A006 Airfoil Sections. NACA RM L50F16, 1950.

17. Katz, Ellis R., and Stoney, William E., Jr.: Base Pressures Measured on Several Parabolic-Arc Bodies of Revolution in Free Flight at Mach Numbers From 0.8 to 1.4 and at Large Reynolds Numbers. NACA RM L51F29, 1951.

[redacted]

TABLE I

ORDINATES FOR THE FUSELAGE AND FOR THE NACA 65A006 AIRFOIL SECTION

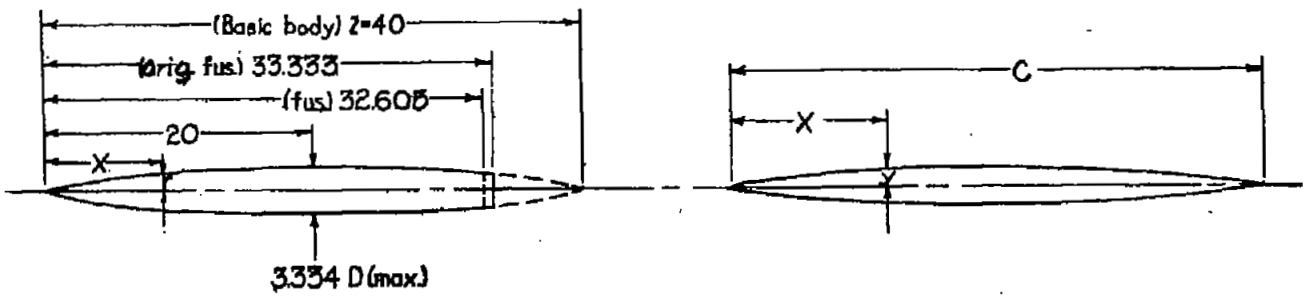

FUSELAGE ORDINATES			
x/l	r/l	x/l	r/l
0	0	0.4500	0.04143
.0050	.00231	.5000	.04167
.0075	.00298	.5500	.04130
.0125	.00428	.6000	.04024
.0250	.00722	.6500	.03842
.0500	.01205	.7000	.03562
.0750	.01613	.7500	.03128
.1000	.01971	.8000	.02526
.1500	.02593	.8151	.02326
.2000	.03090	.8333	.02083
.2500	.03465	.8500	.01852
.3000	.03741	.9000	.01125
.3500	.03933	.9500	.00439
.4000	.04063	1.0000	0

L.E. radius = 0.0005l
c/4 located at D(max.)

Fineness ratio
Original fuselage 10.0
Fuselage 9.8

AIRFOIL ORDINATES			
x/c	y/c	x/c	y/c
0	0	0.40	0.02996
.005	.00464	.45	.02992
.0075	.00563	.50	.02925
.0125	.00718	.55	.02793
.025	.00981	.60	.02602
.050	.01313	.65	.02364
.075	.01591	.70	.02087
.10	.01824	.75	.01775
.15	.02194	.80	.01437
.20	.02474	.85	.01083
.25	.02687	.90	.00727
.30	.02842	.95	.00370
.35	.02945	1.00	.00013

L.E. radius = 0.0022c T.E. radius = 0.0001$4c$

TABLE II

INDEX OF FIGURES PRESENTING RESULTS

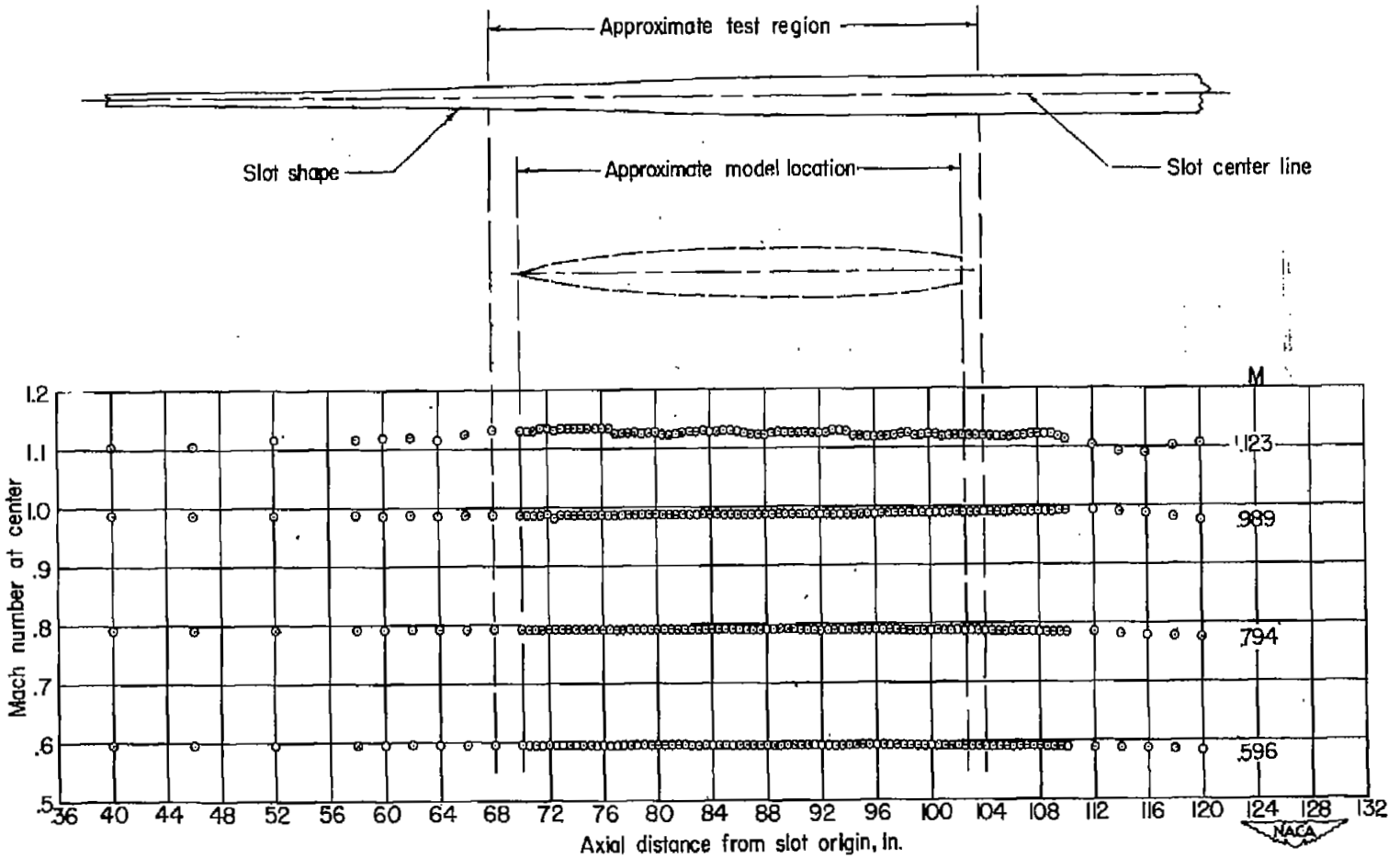

Figure 1.- Typical Mach number distributions in the test section of the Langley 8-foot transonic tunnel.

Figure 2.- Model as tested in the Langley 8-foot transonic tunnel.

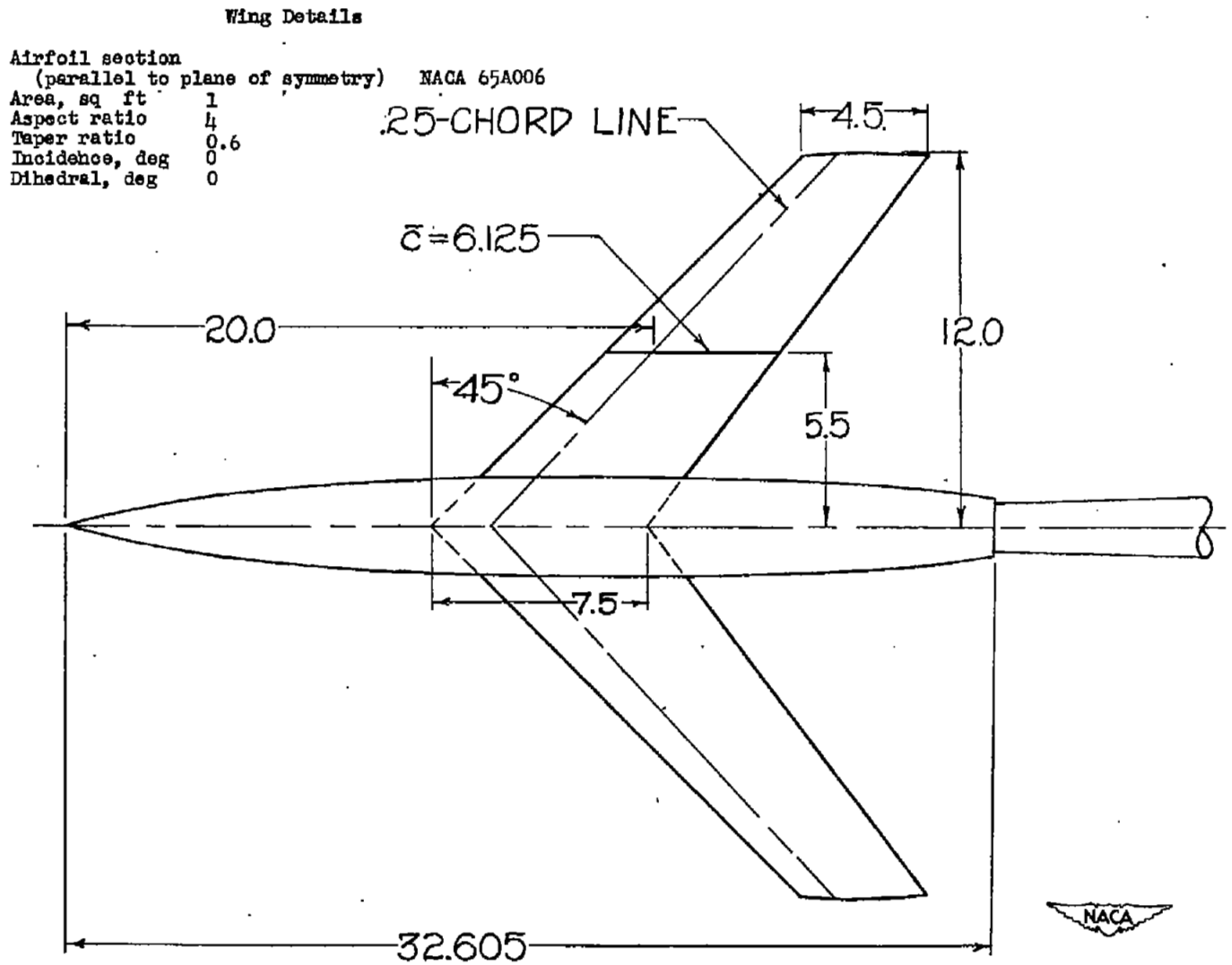

Figure 3.- Model details. All dimensions in inches unless otherwise noted.

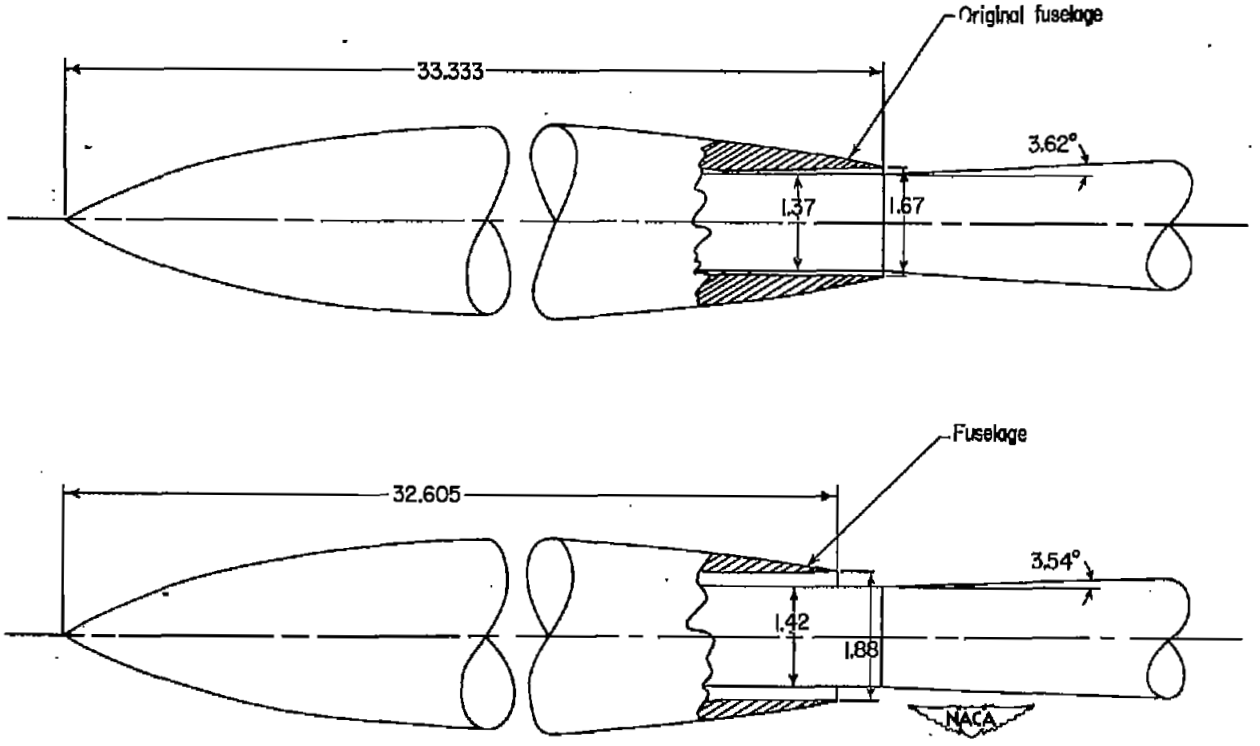

Original fuselage		Fuselage	
$\frac{\text{Diameter of sting at model base}}{\text{Diameter of model base}}$	=0.820	$\frac{\text{Diameter of sting at model base}}{\text{Diameter of model base}}$	=0.755
$\frac{\text{Area of model base}}{\text{Area of wing}}$	=0.015	$\frac{\text{Area of model base}}{\text{Area of wing}}$	=0.019

Figure 4.- Details of model base for the original fuselage and the fuselage configurations. All dimensions in inches unless otherwise noted.

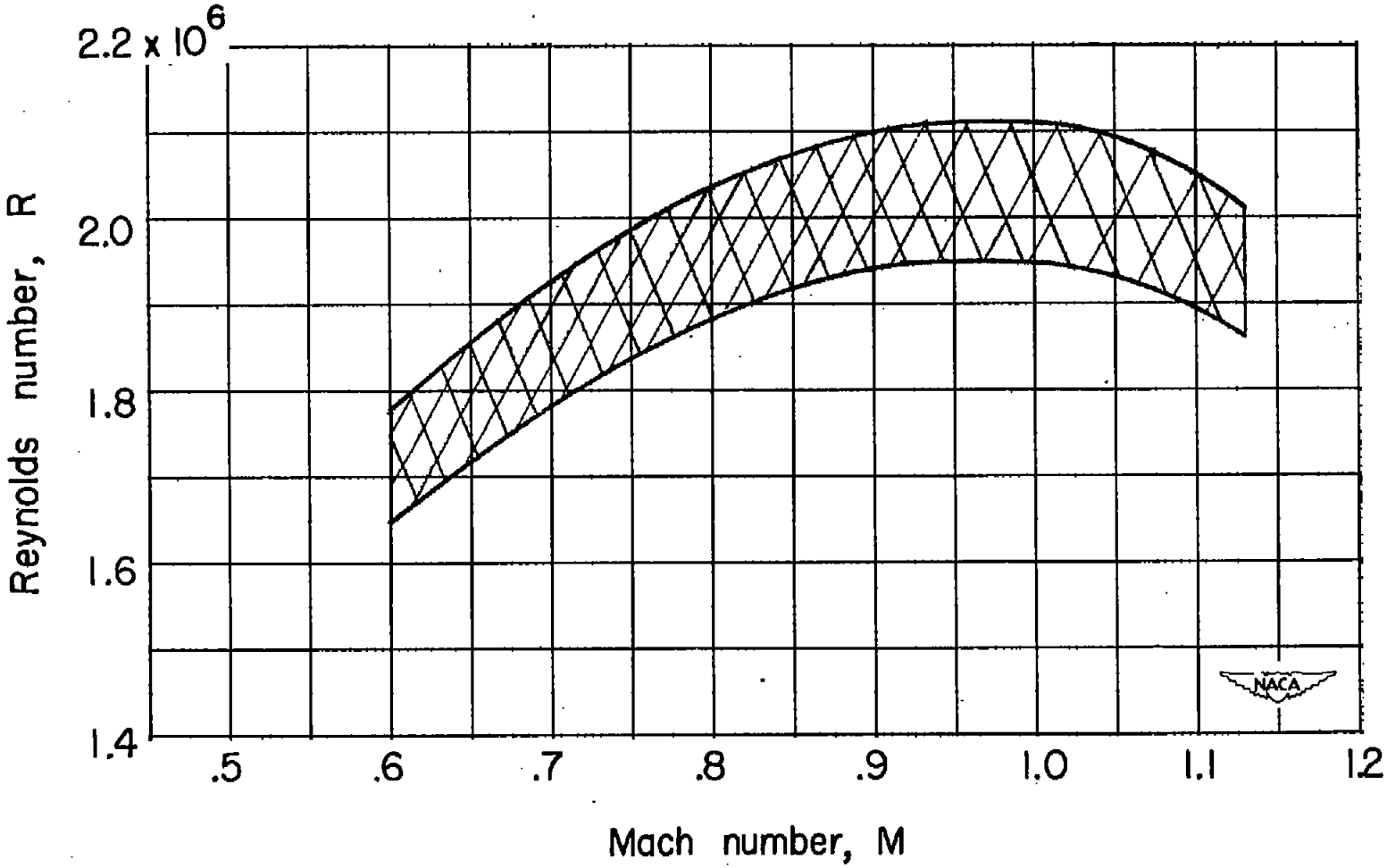

Figure 6.- Variation with Mach number of test Reynolds number based on $\bar{c}$ = 6.125 inches.

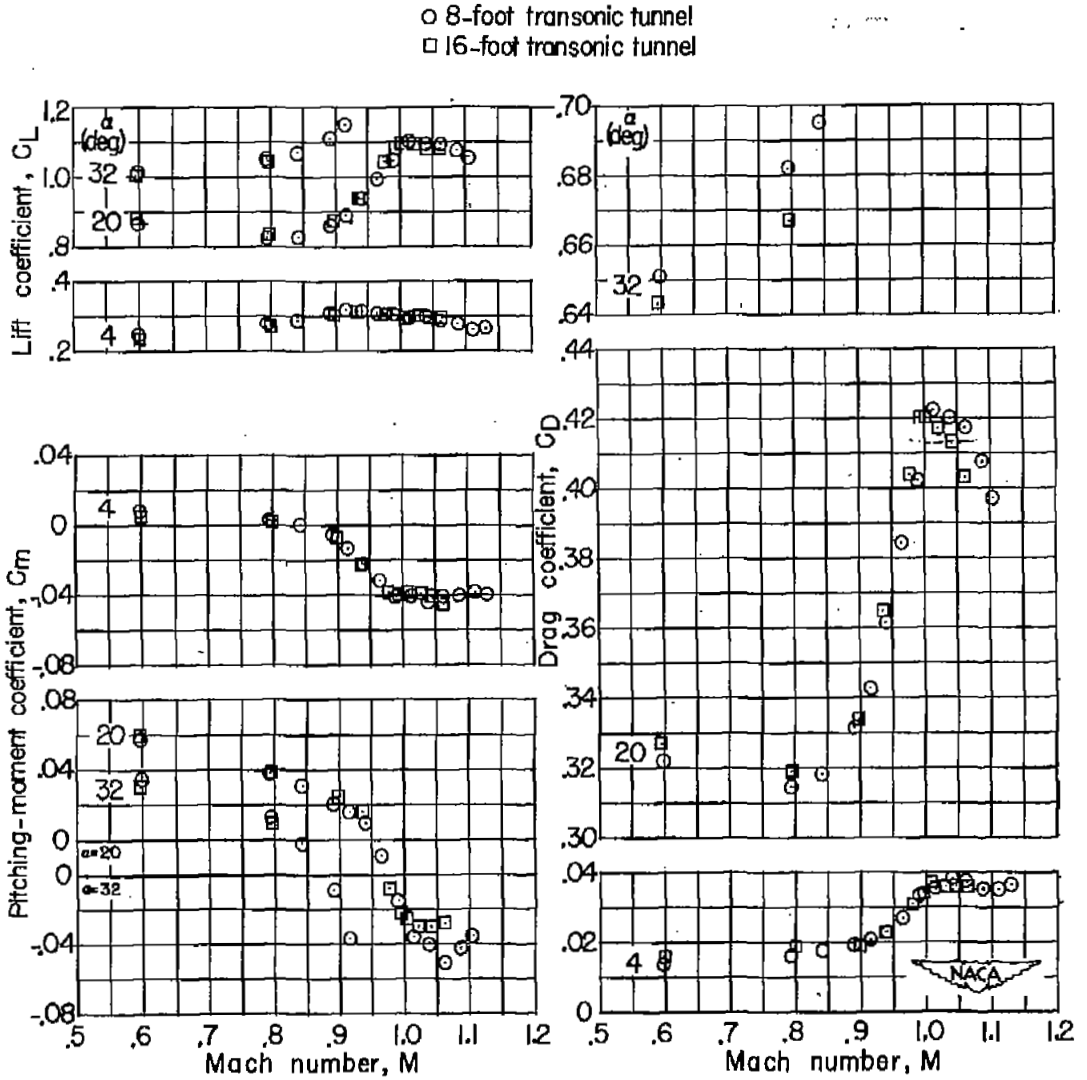

Figure 7.- Comparison of aerodynamic characteristics for the wing-fuselage configuration obtained in the Langley 8-foot and 16-foot transonic tunnels.

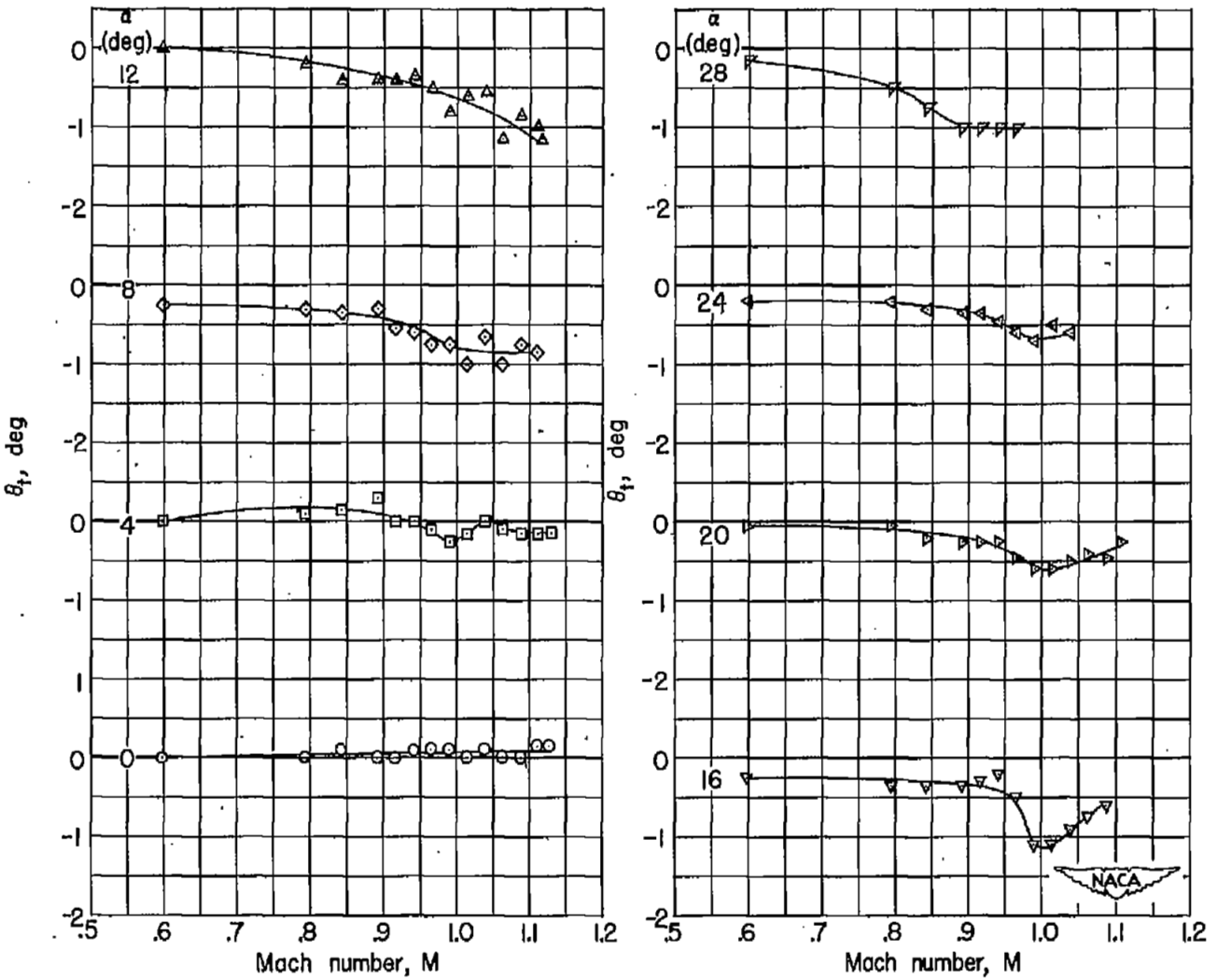

Figure 8.- Variation with Mach number of the measured angles of wing-tip twist.

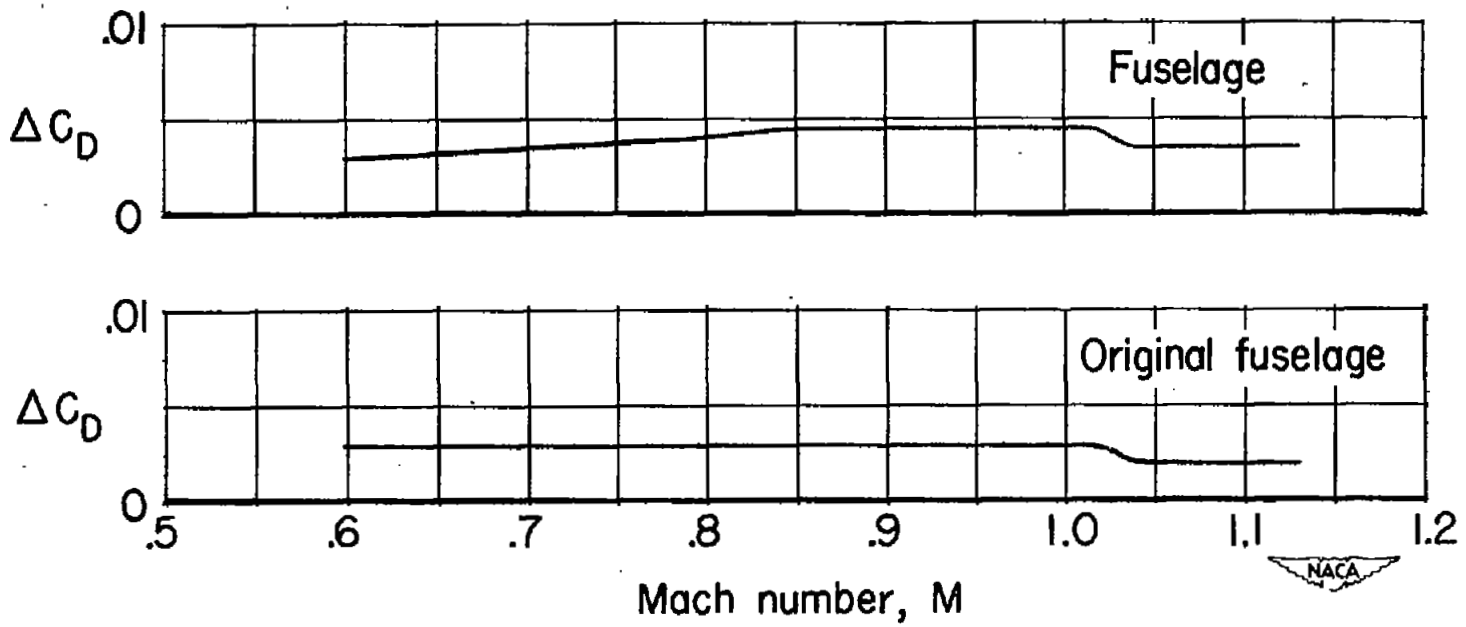

Figure 9.- Variation with Mach number of the decrease in drag coefficient due to sting interference for configurations employing the original fuselage and the fuselage.

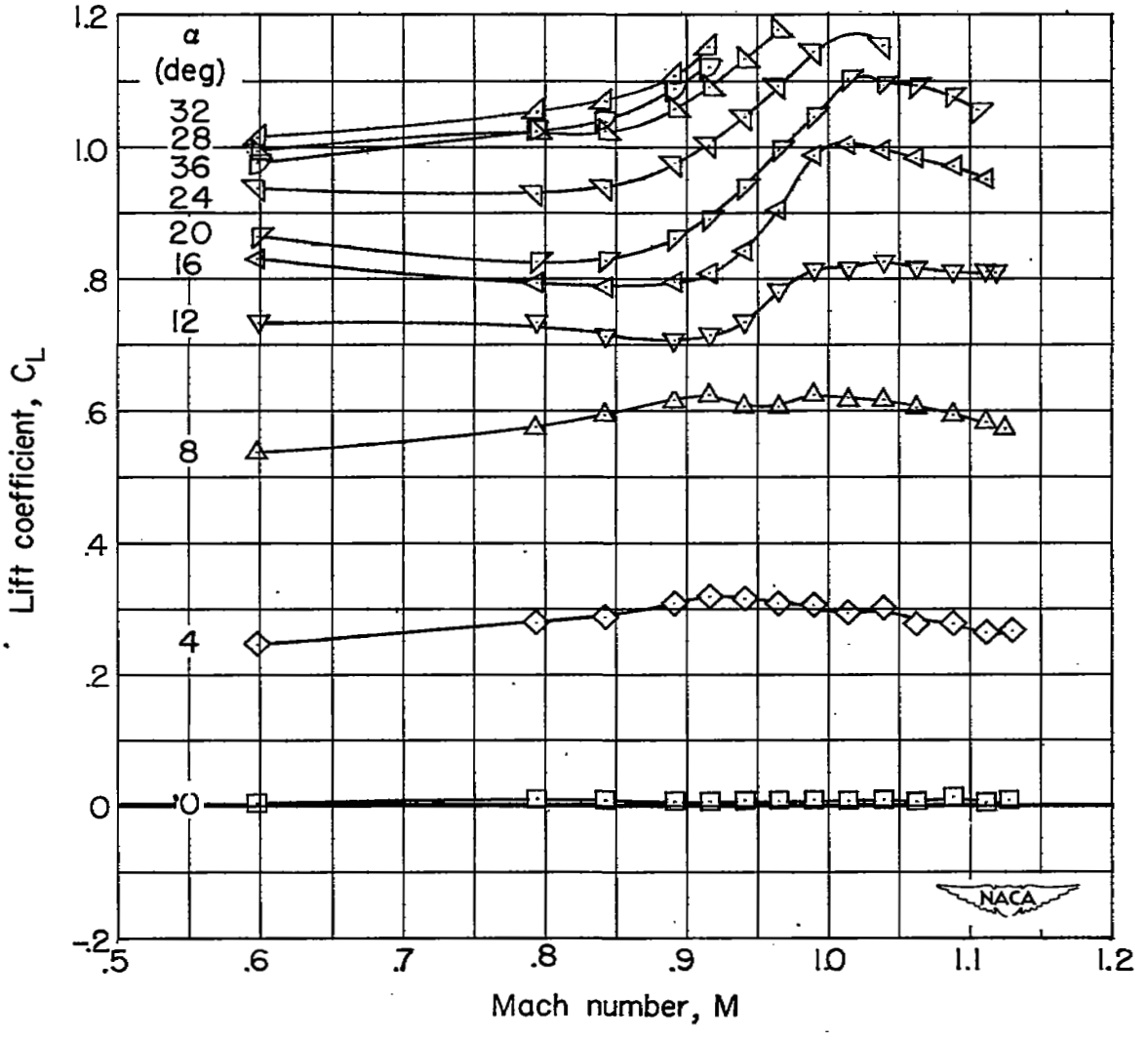

(a) Lift coefficient.

Figure 10.- Variation with Mach number of the force and moment characteristics of the wing-fuselage configuration.

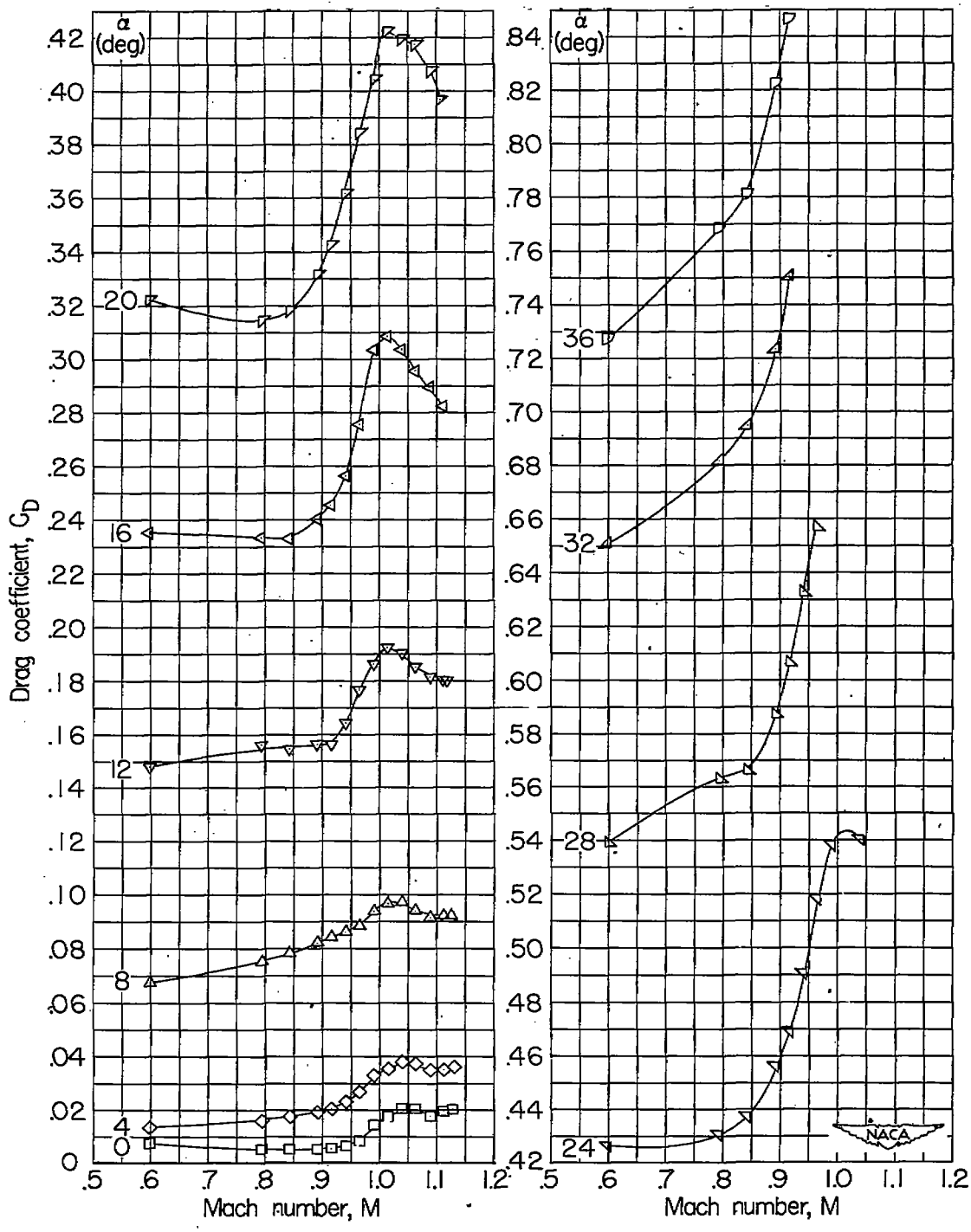

(b) Drag coefficient.

Figure 10.- Continued.

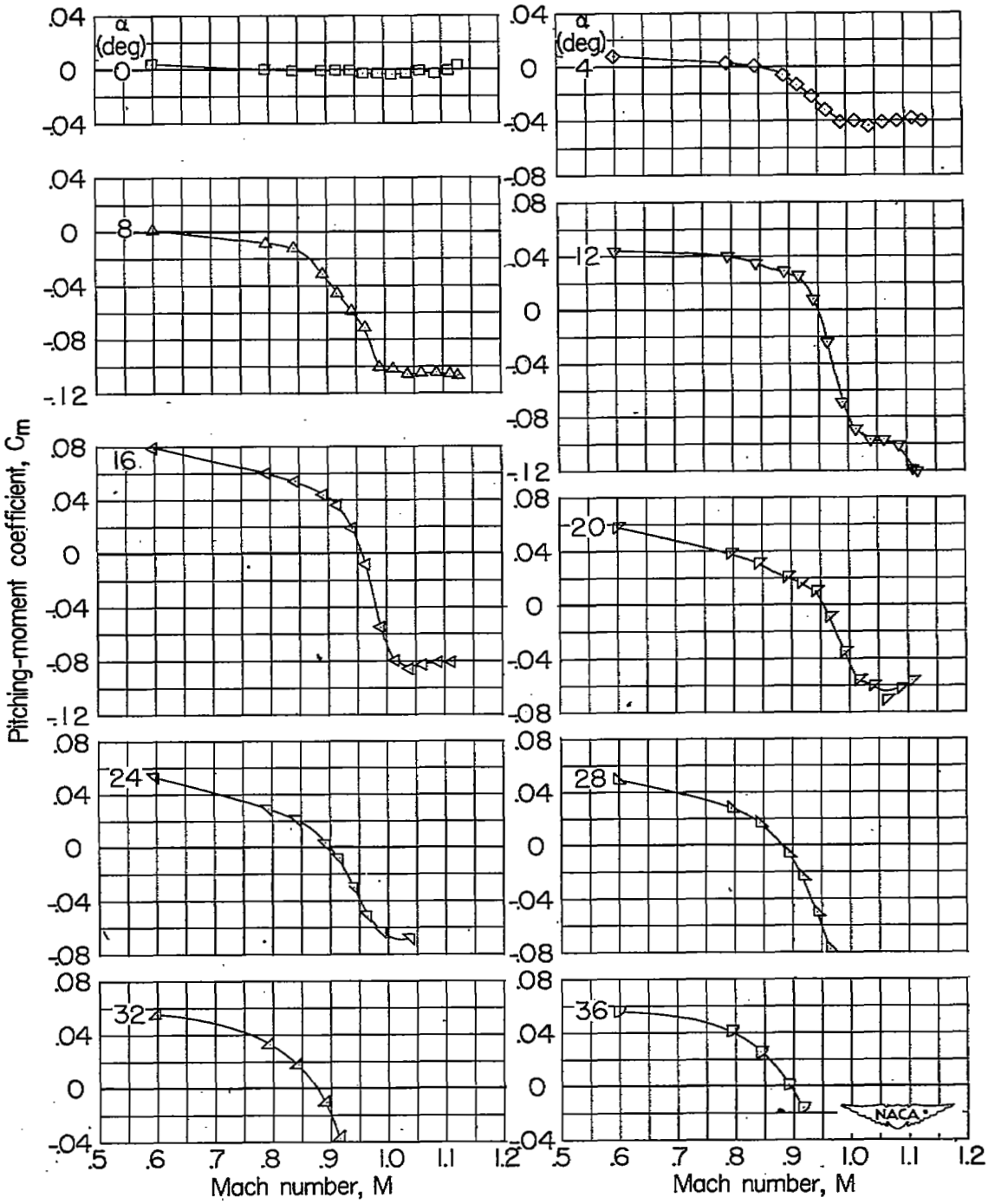

(c) Pitching-moment coefficient.

Figure 10.- Concluded.

[redacted]

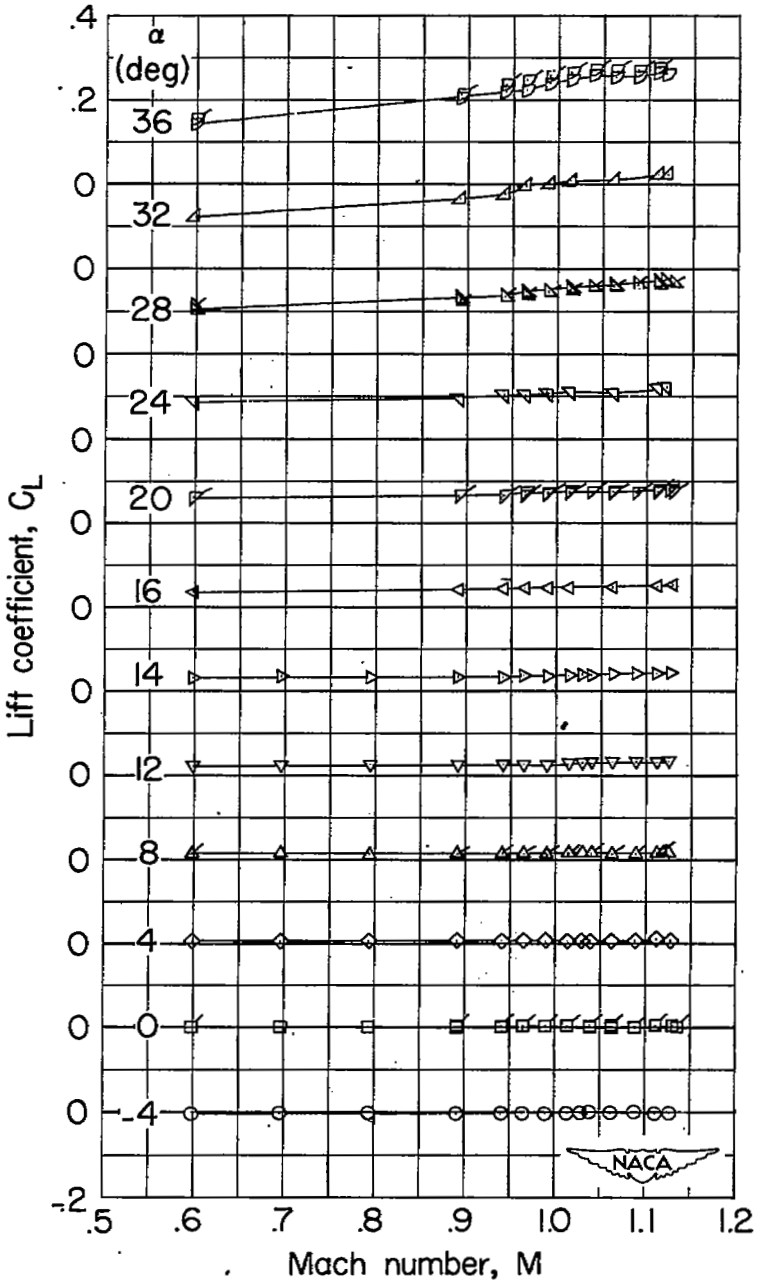

(a) Lift coefficient.

Figure 11.- Variation with Mach number of the force and moment characteristics of the original fuselage and fuselage configurations. Flagged symbols denote data for the fuselage configuration.

[redacted]

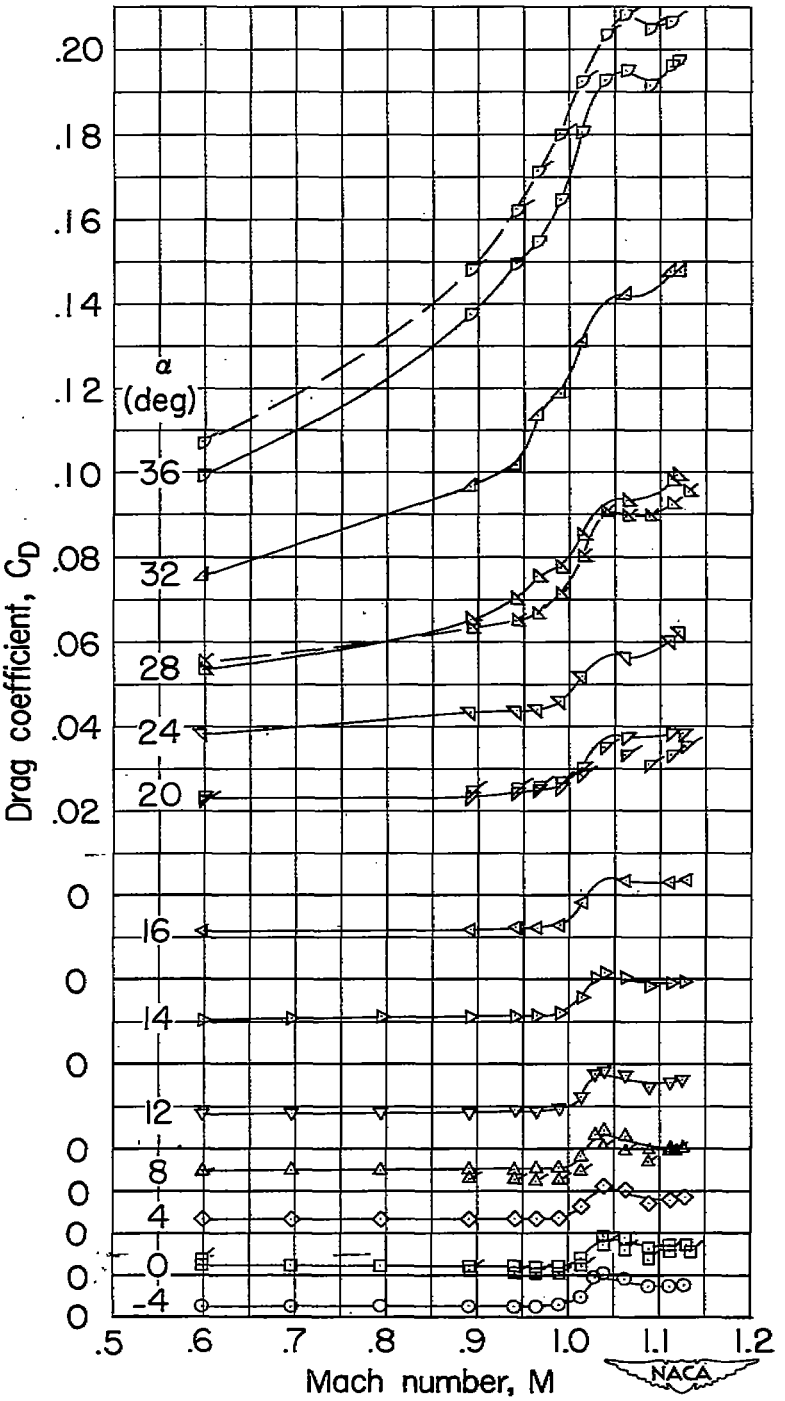

(b) Drag coefficient.

Figure 11.- Continued.

[redacted]

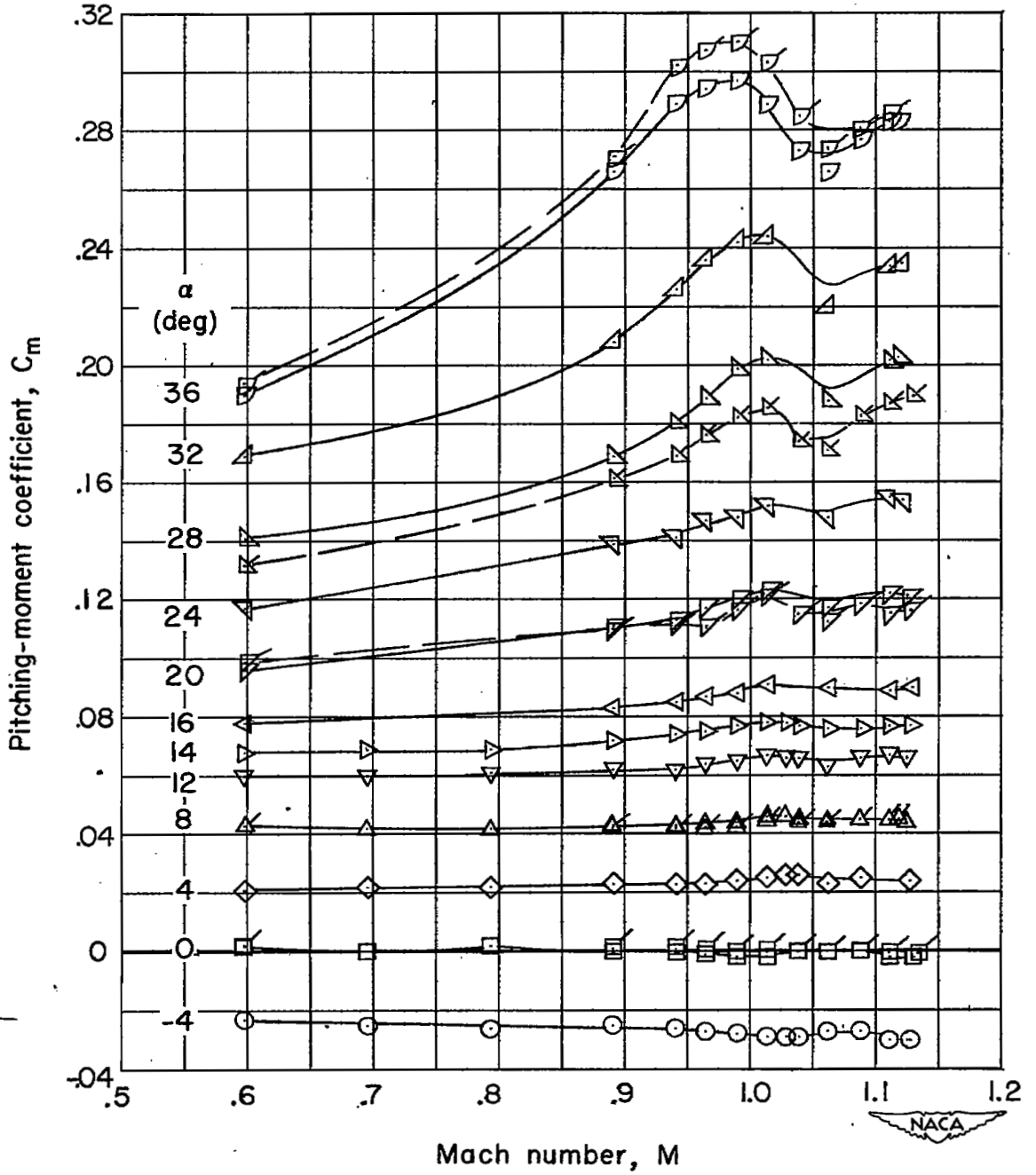

(c) Pitching-moment coefficient.

Figure 11.- Concluded.

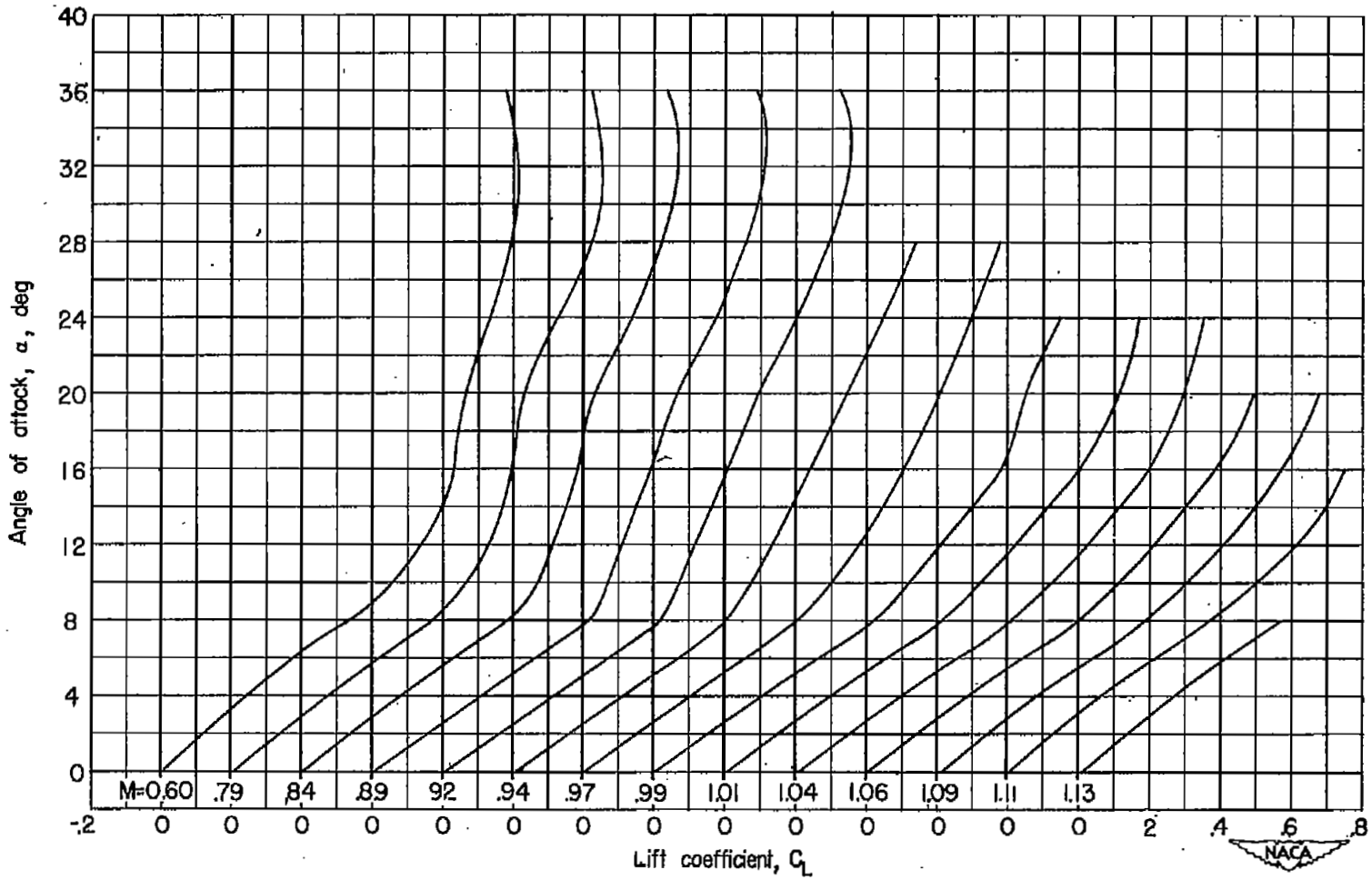

(a) Angle of attack.

Figure 12.- Variation with lift coefficient of the force and moment characteristics of the wing-fuselage configuration.

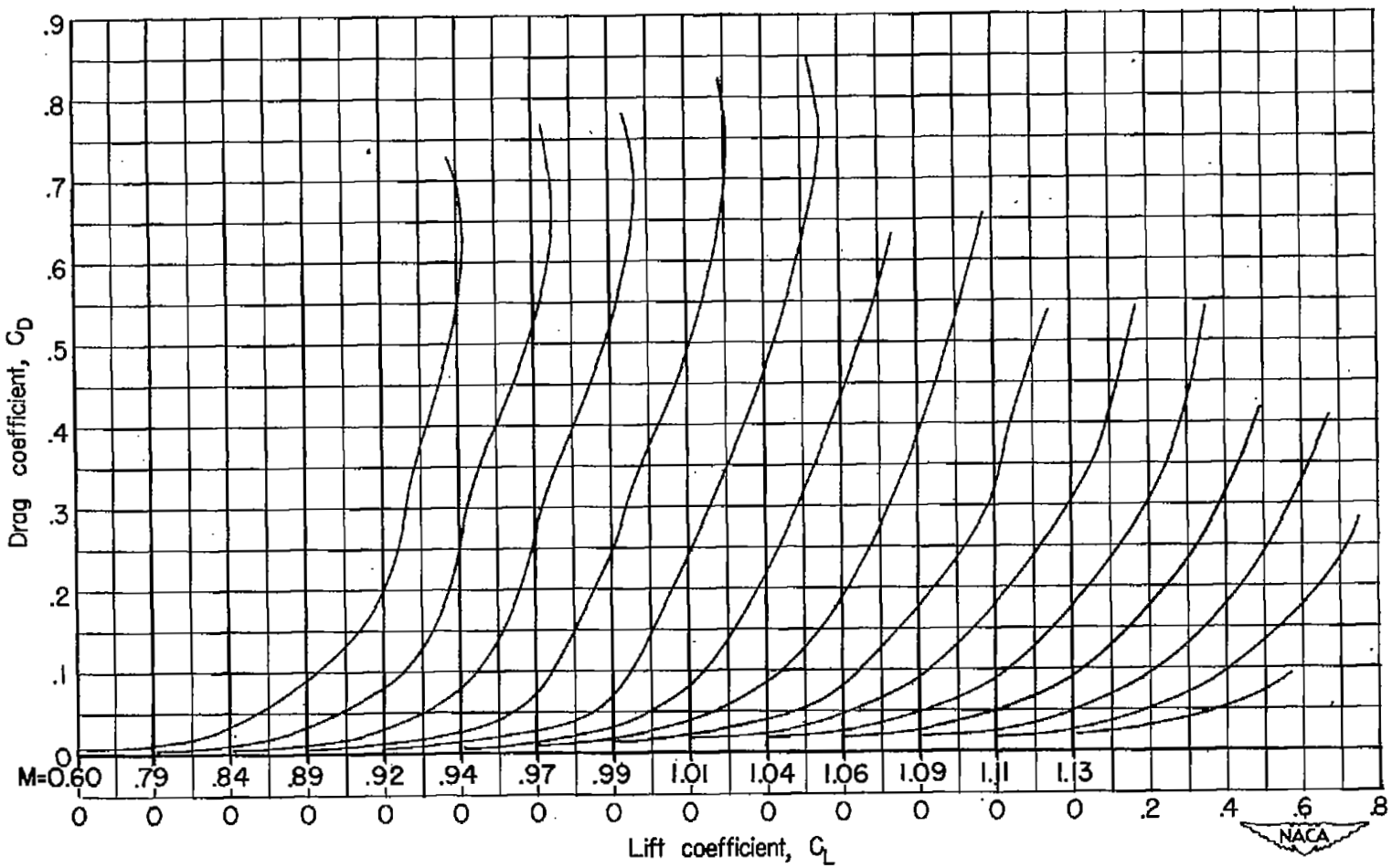

(b) Drag coefficient.

Figure 12.- Continued.

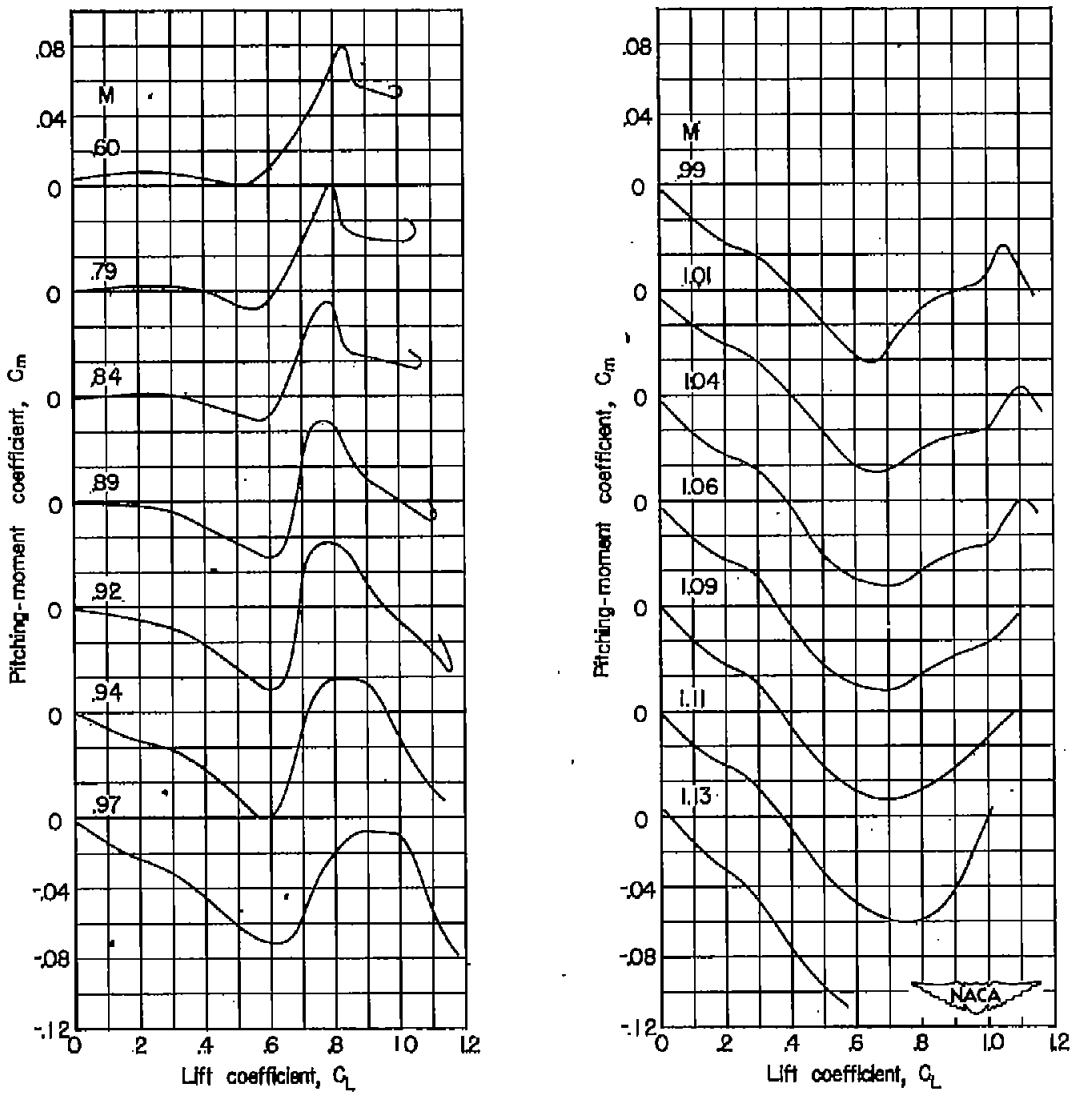

(c) Pitching-moment coefficient.

Figure 12.- Concluded.

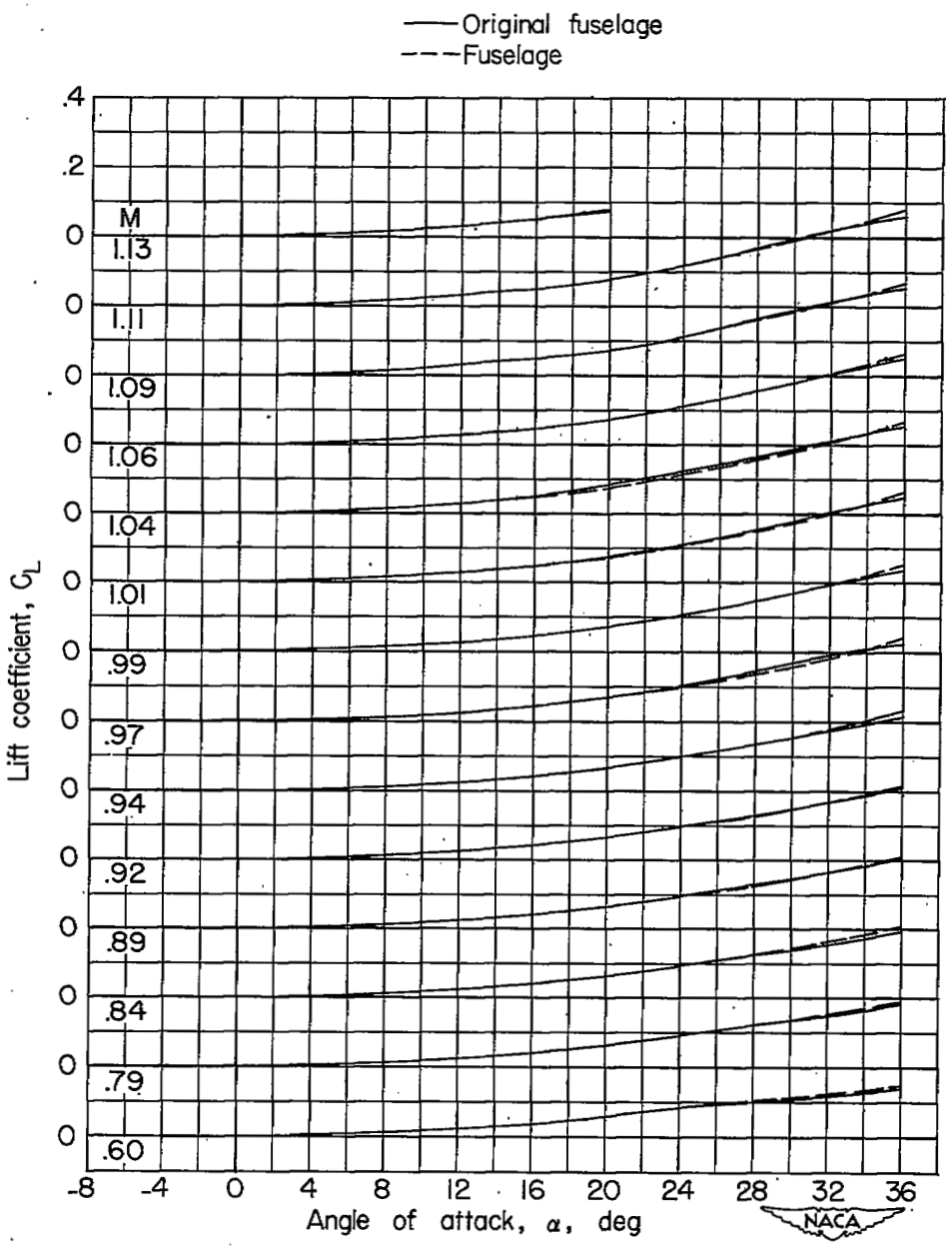

(a) Lift coefficient.

Figure 13.- Variation with angle of attack of the force and moment characteristics of the original fuselage and fuselage configurations.

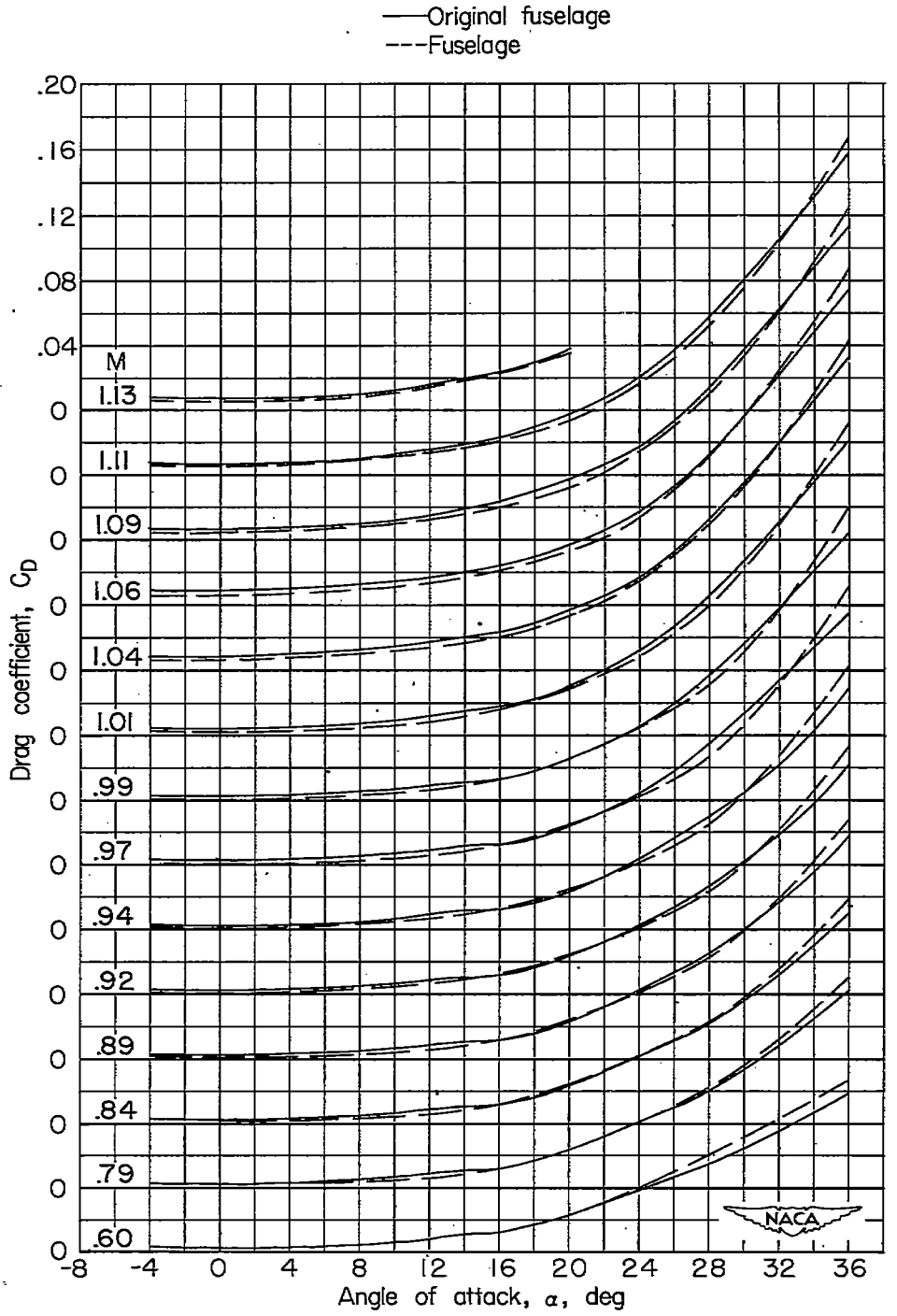

(b) Drag coefficient.

Figure 13.- Continued.

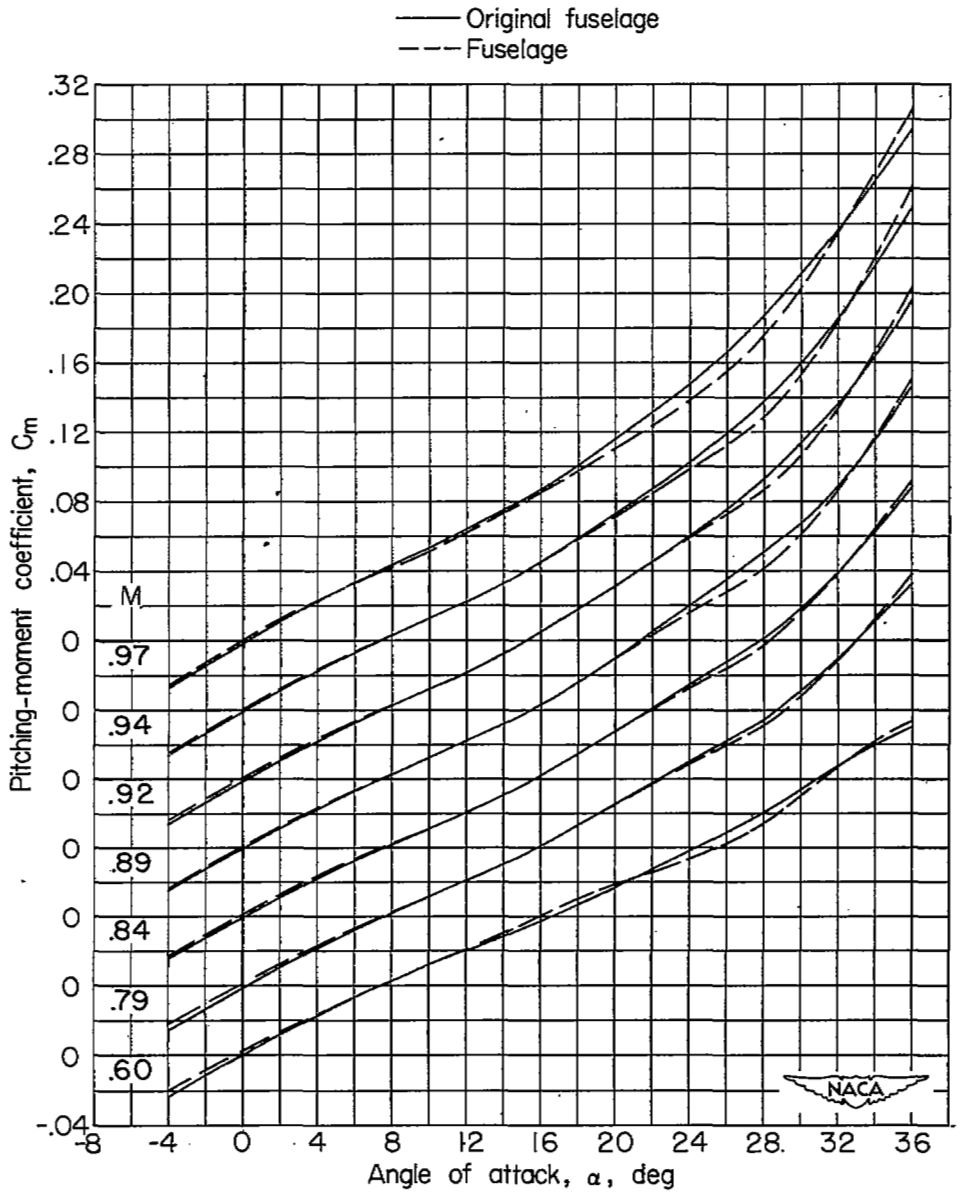

(c) Pitching-moment coefficient.

Figure 13.- Continued.

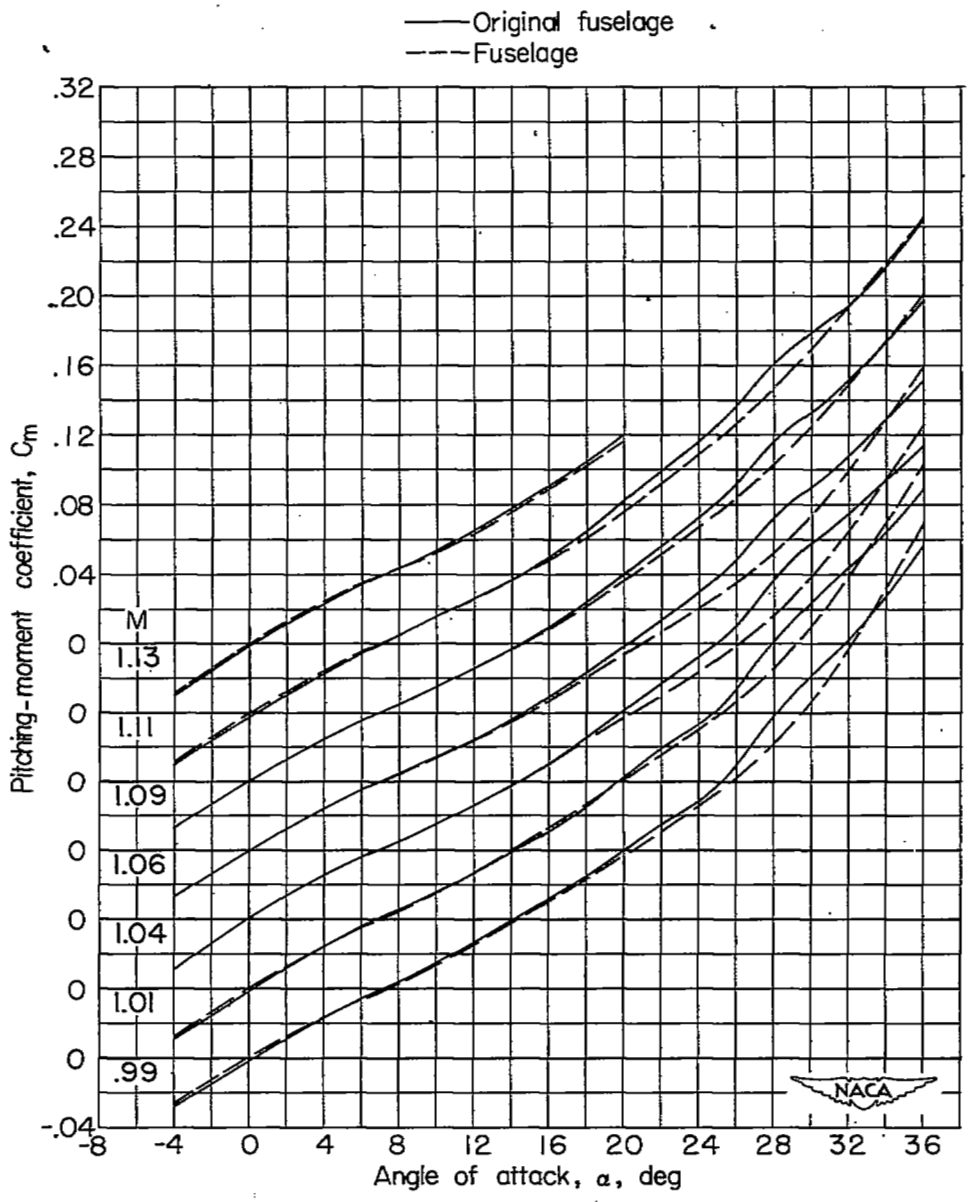

(c) Pitching-moment coefficient. Concluded.

Figure 13.- Concluded.

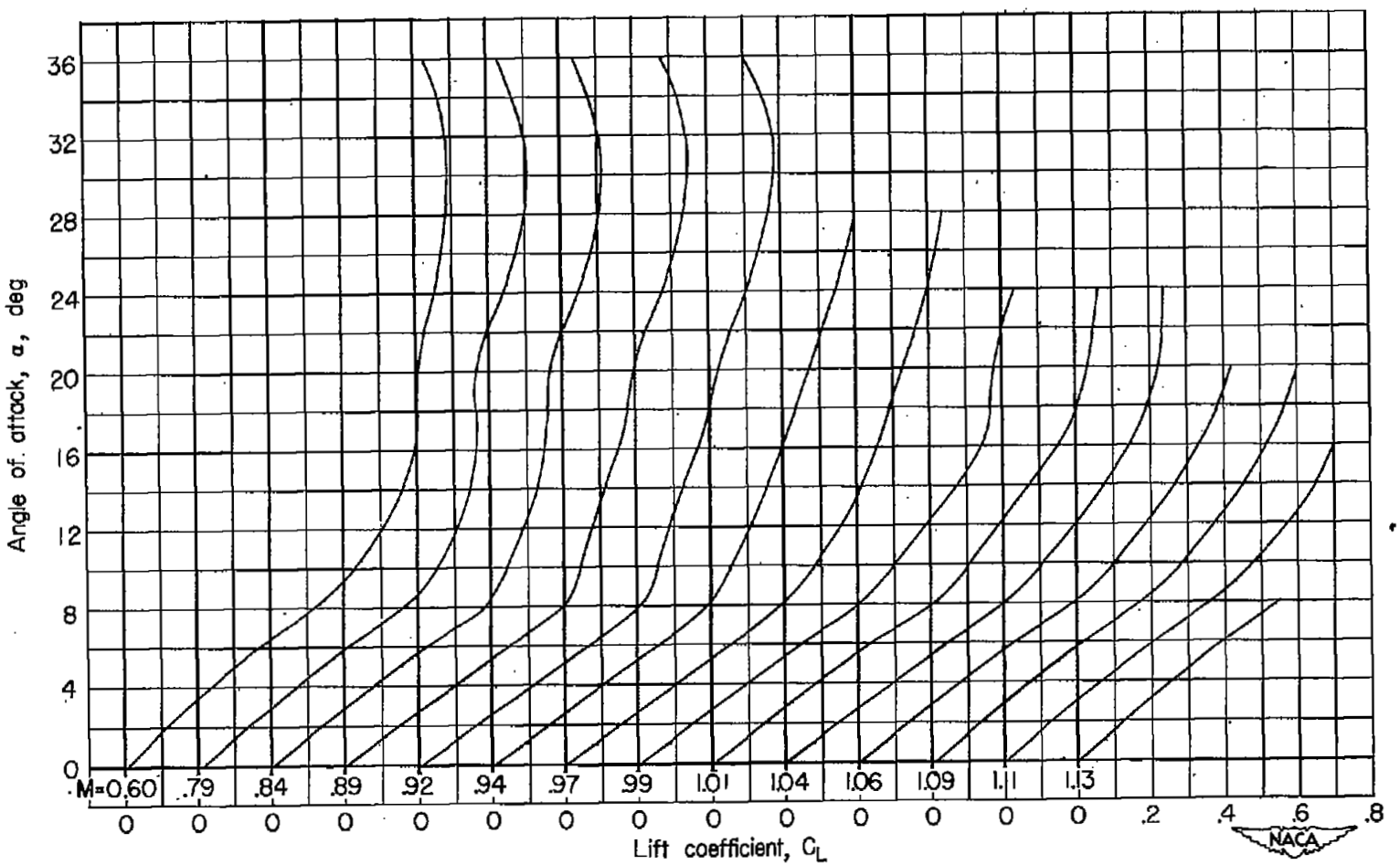

(a) Angle of attack.

Figure 14.- Variation with lift coefficient of the force and moment characteristics of the wing with interference.

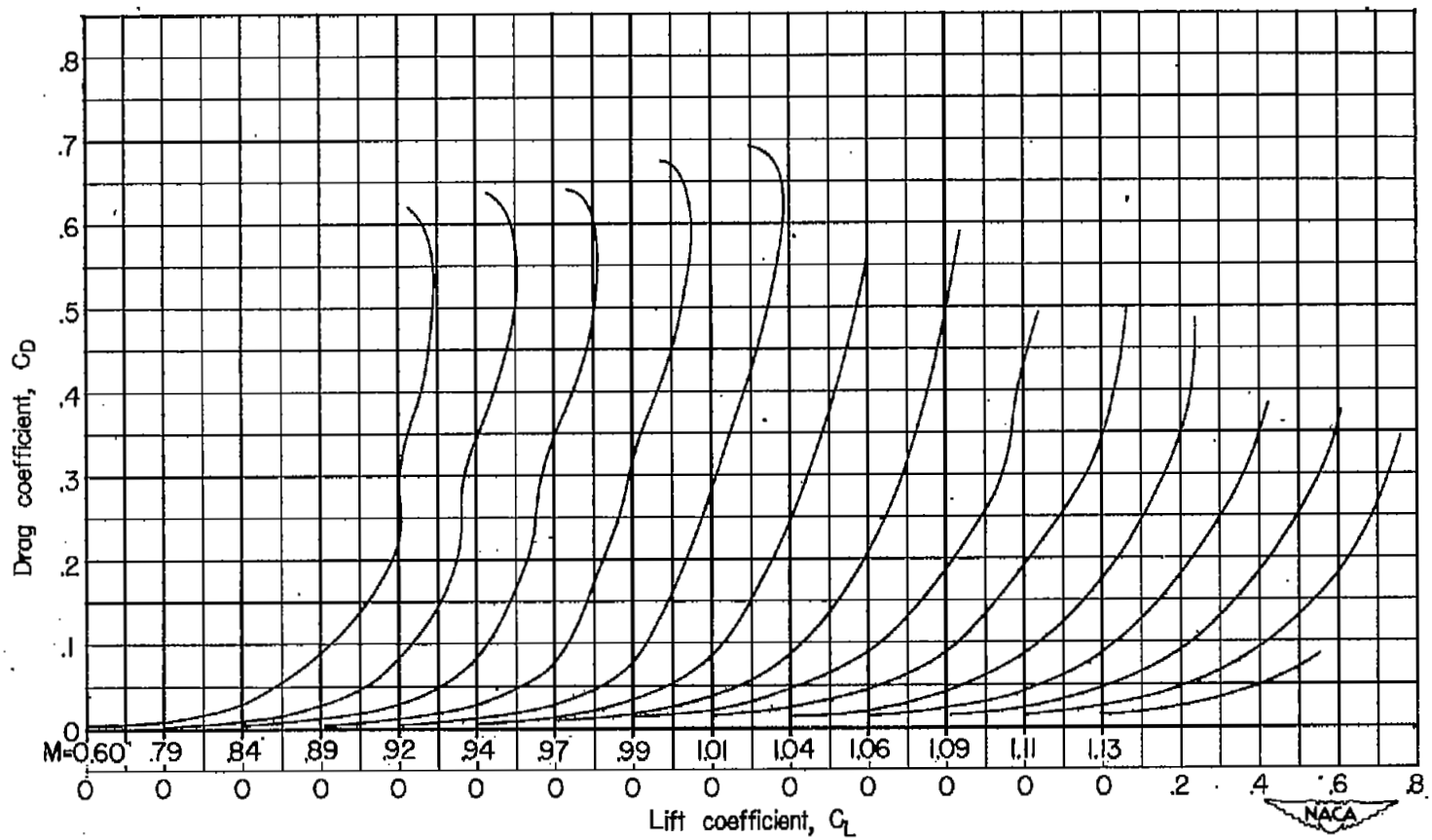

(b) Drag coefficient.

Figure 14.- Continued.

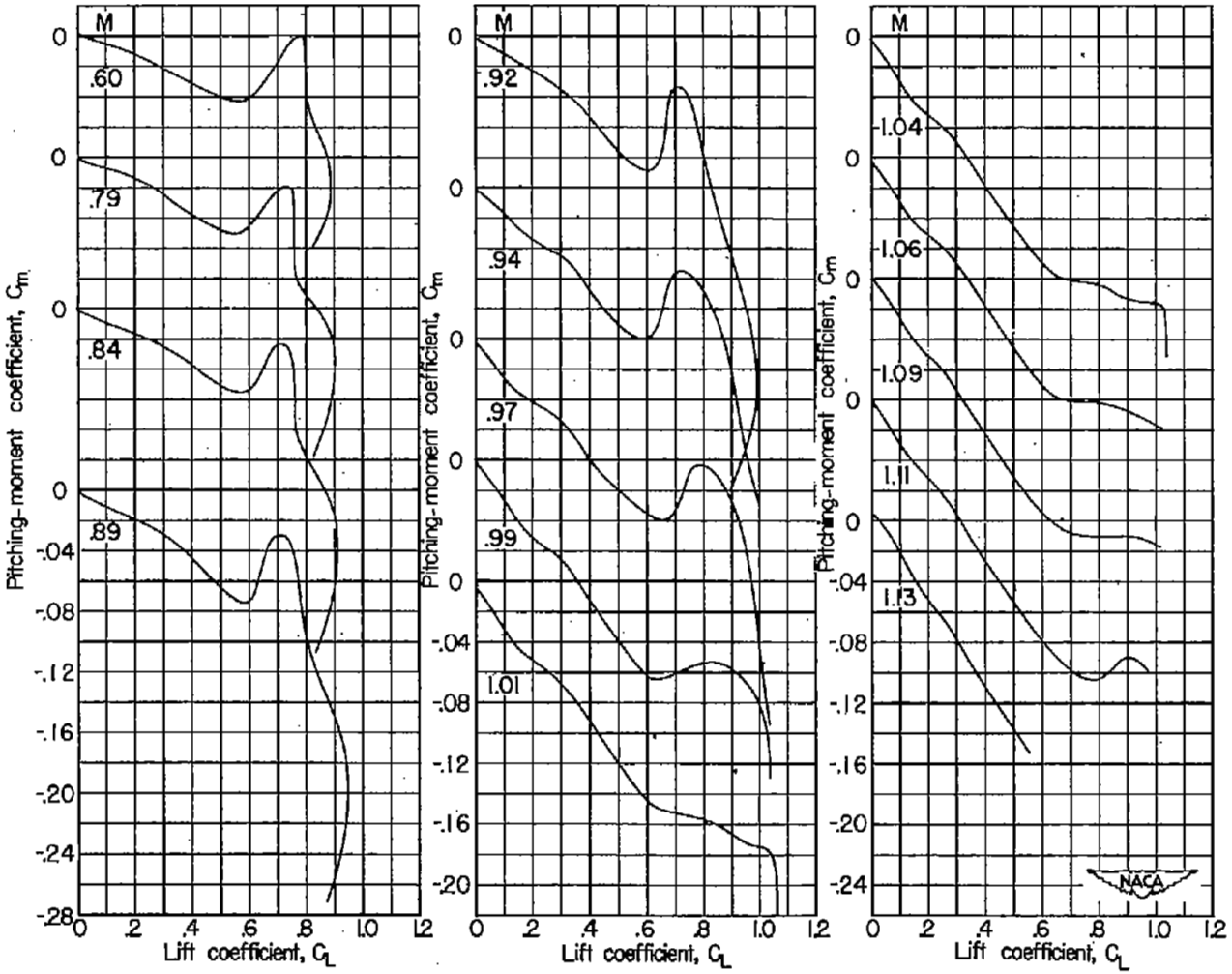

(c) Pitching-moment coefficient.

Figure 14.- Concluded.

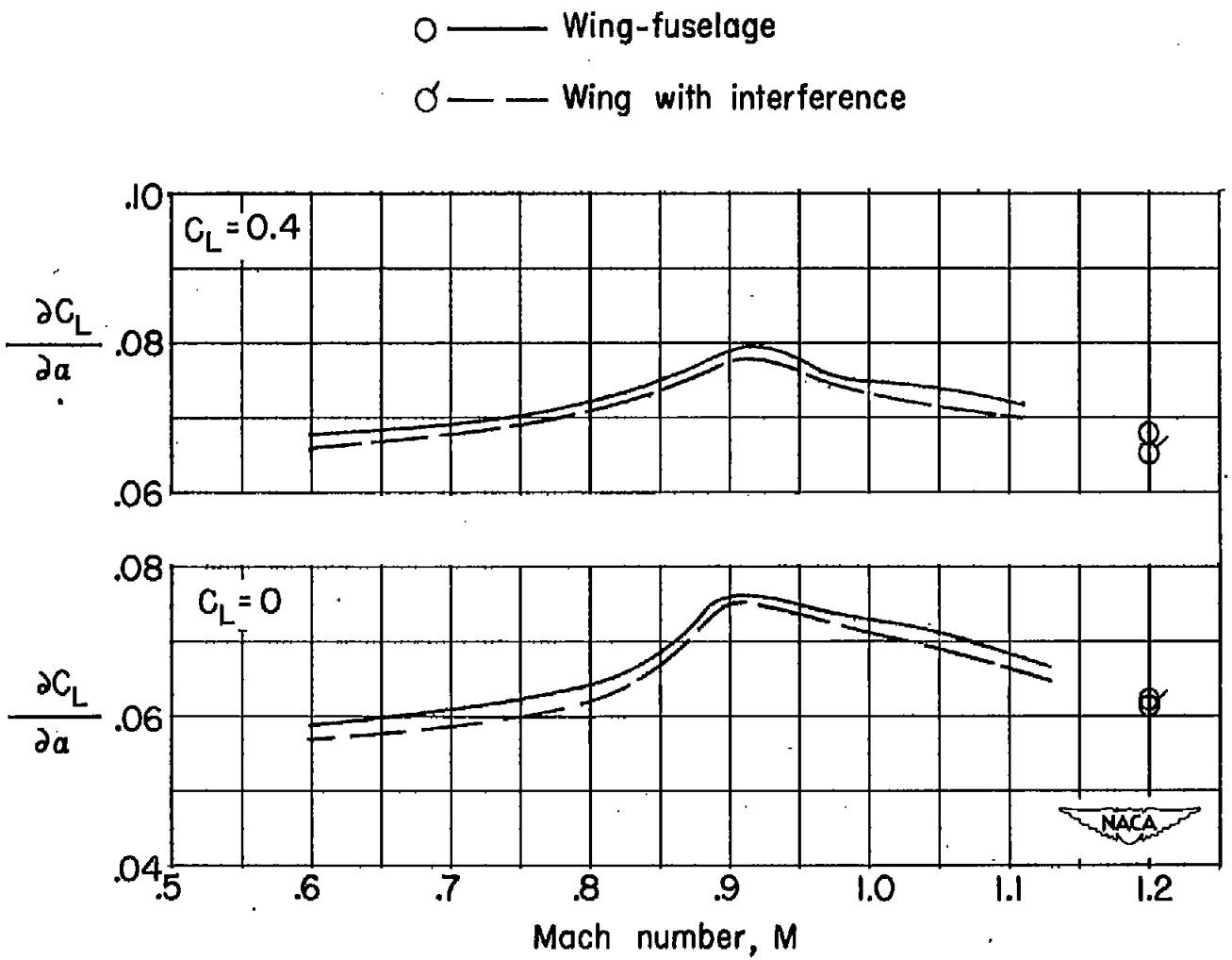

Figure 15.- Variation with Mach number of lift-curve slope for the wing-fuselage configuration and for the wing with interference. Data at M = 1.2 from reference 5.

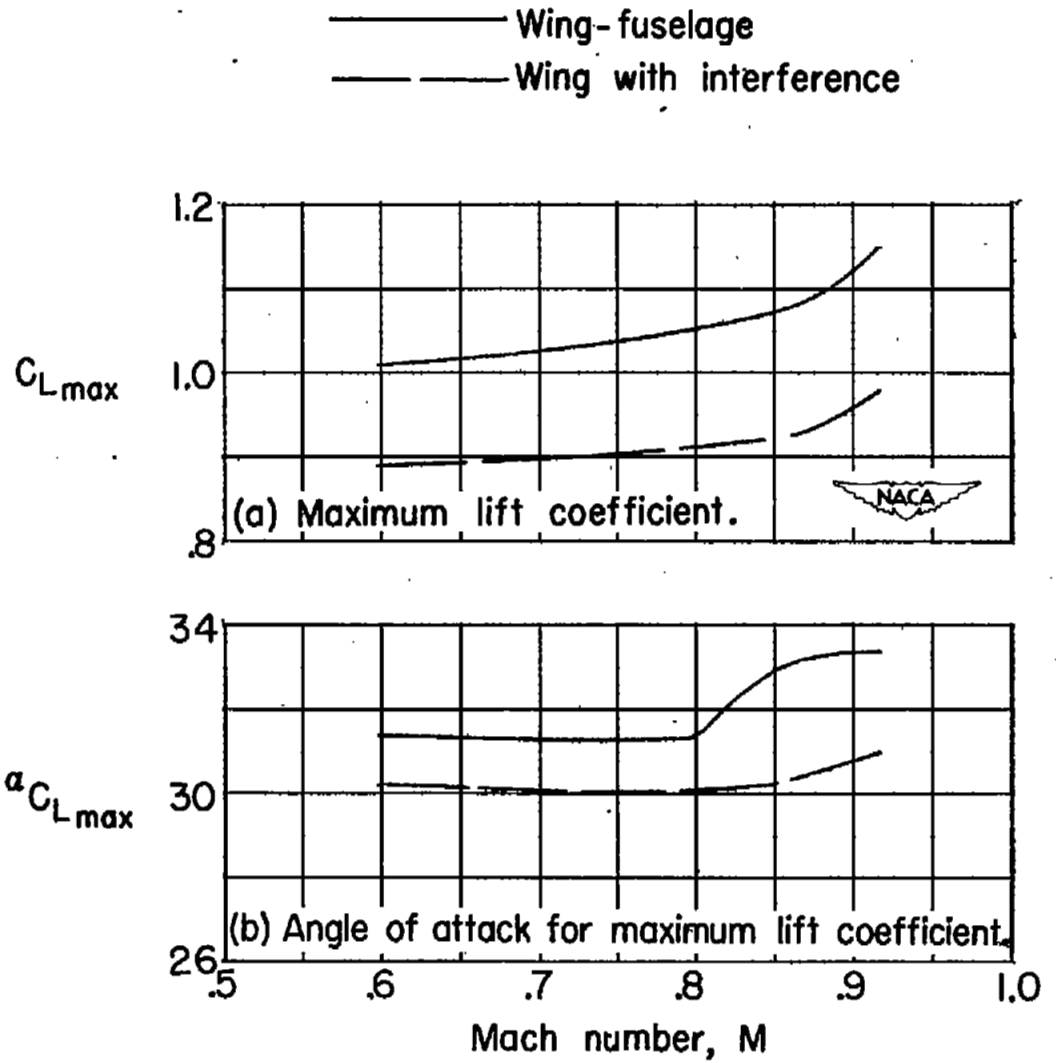

Figure 16.- Variation with Mach number of maximum-lift characteristics of the wing-fuselage configuration and of the wing with interference.

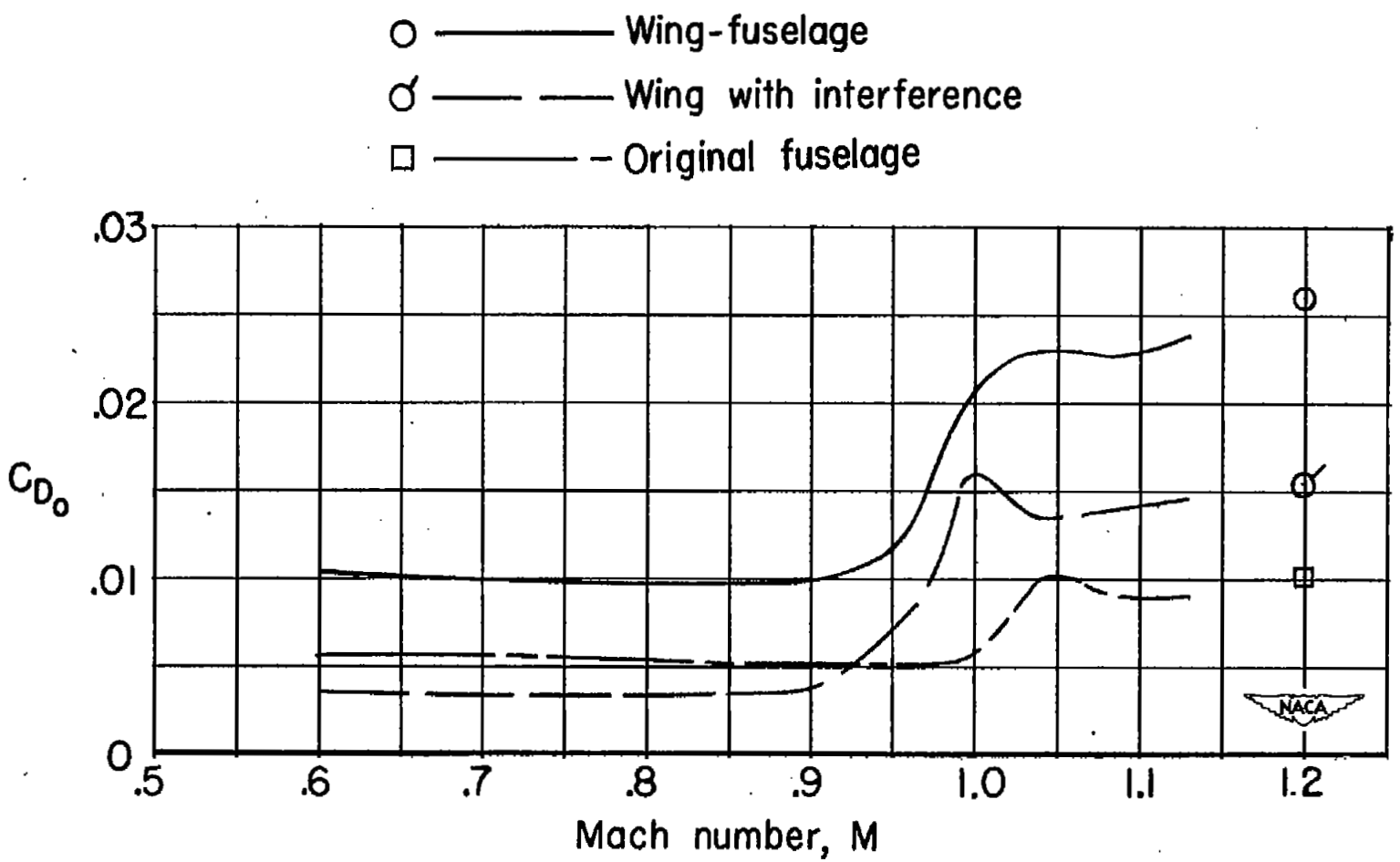

Figure 17.- Variation with Mach number of drag coefficient at zero lift for the wing-fuselage and original fuselage configurations and for the wing with interference. Corrected for sting interference. Data at M = 1.2 from reference 5.

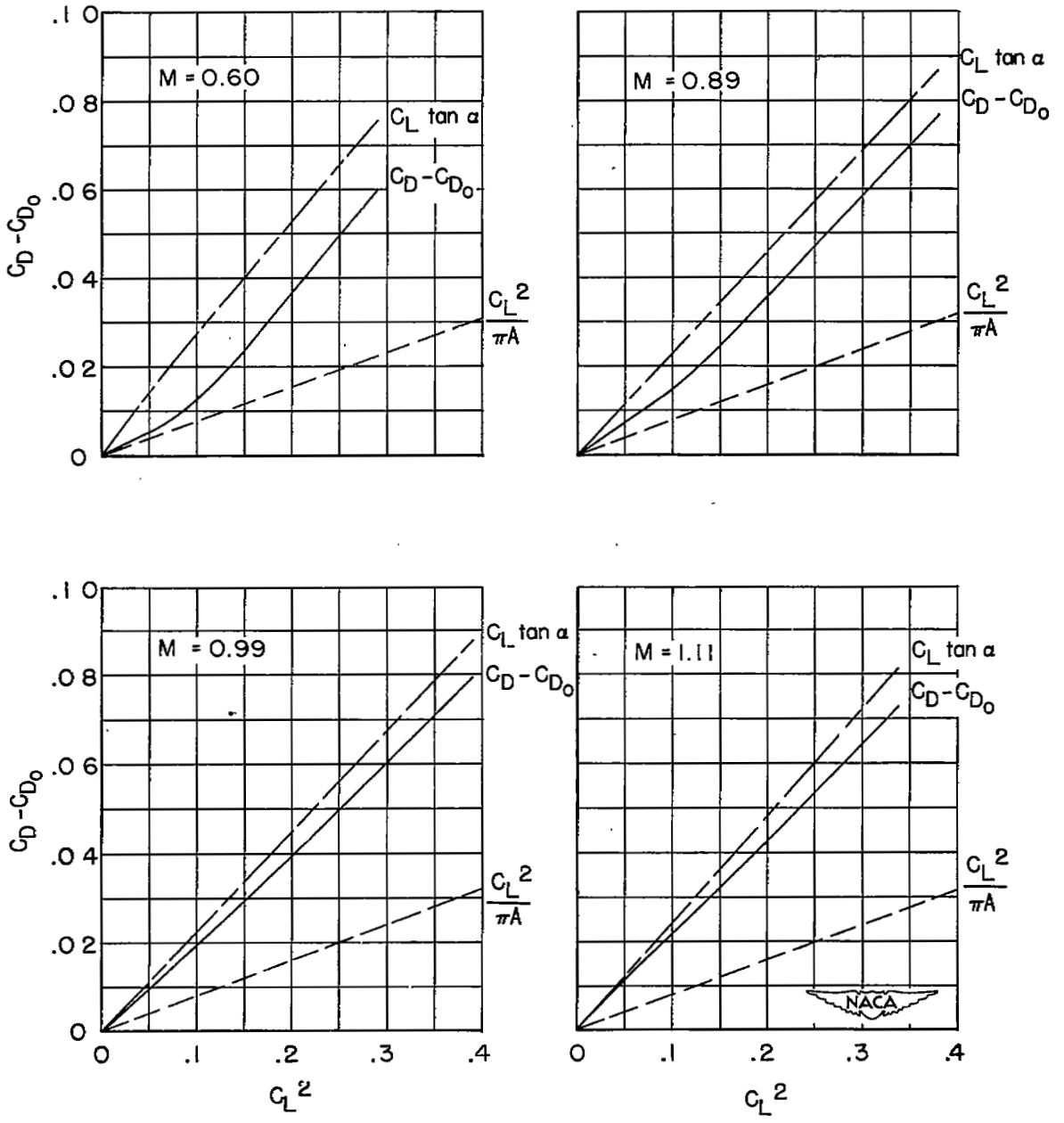

Figure 18.- Variation with lift coefficient squared of drag coefficient due to lift for the wing-fuselage configuration at low lift coefficients.

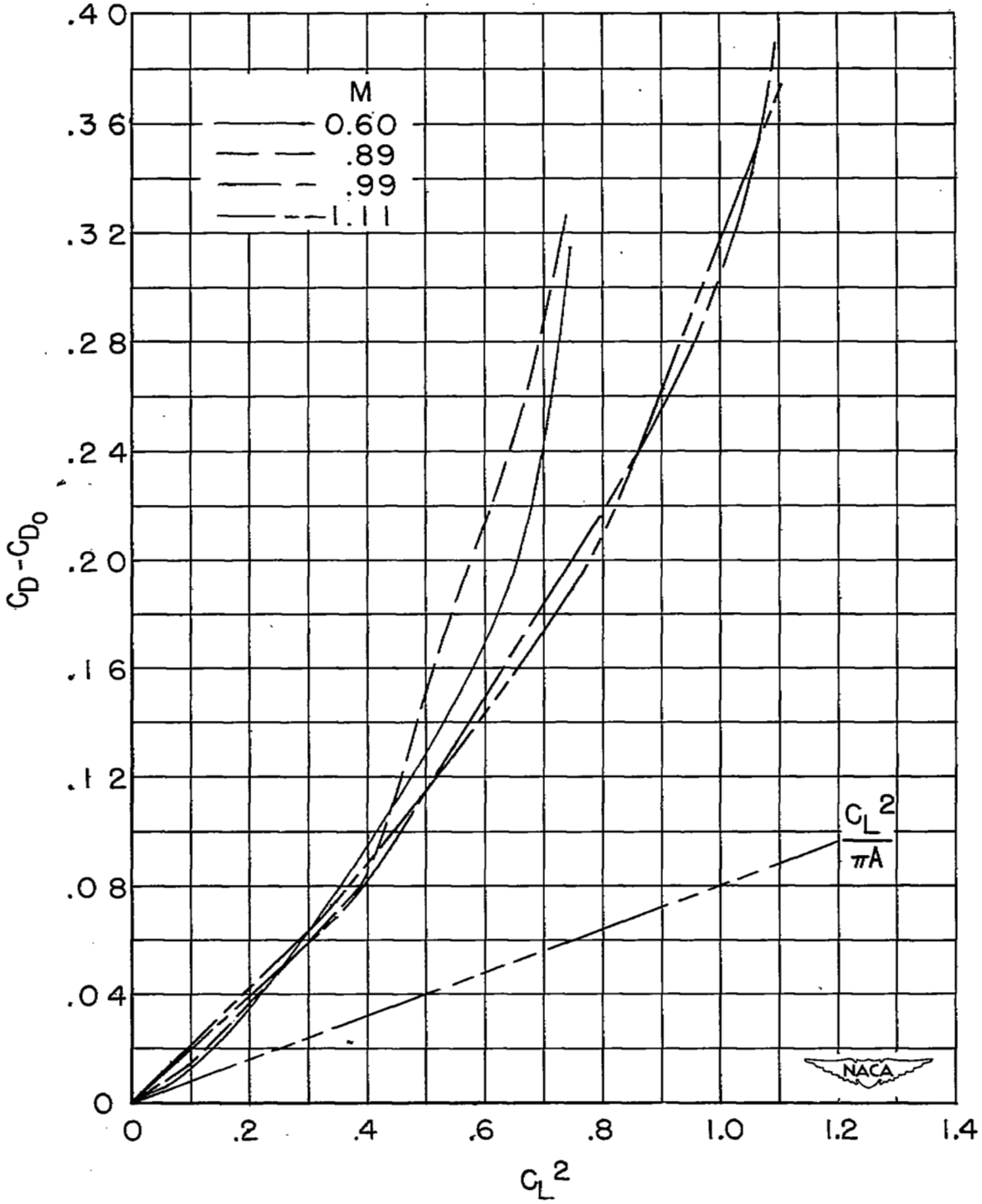

Figure 19.- Variation with lift coefficient squared of drag coefficient due to lift for the wing-fuselage configuration at high lift coefficients.

[redacted]

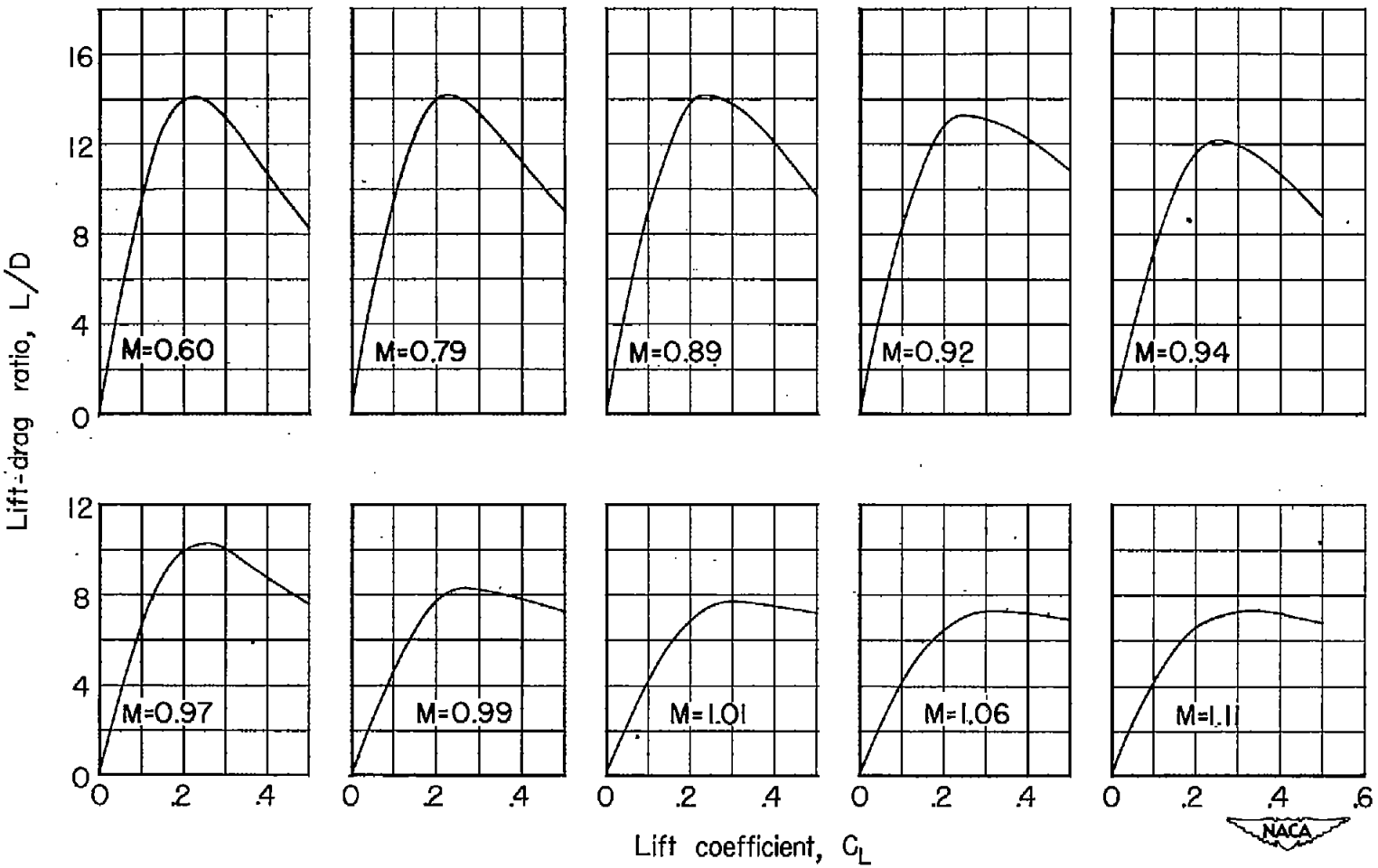

Figure 20.- Variation with lift coefficient of lift-drag ratio for the wing-fuselage configuration. Drag corrected for sting interference.

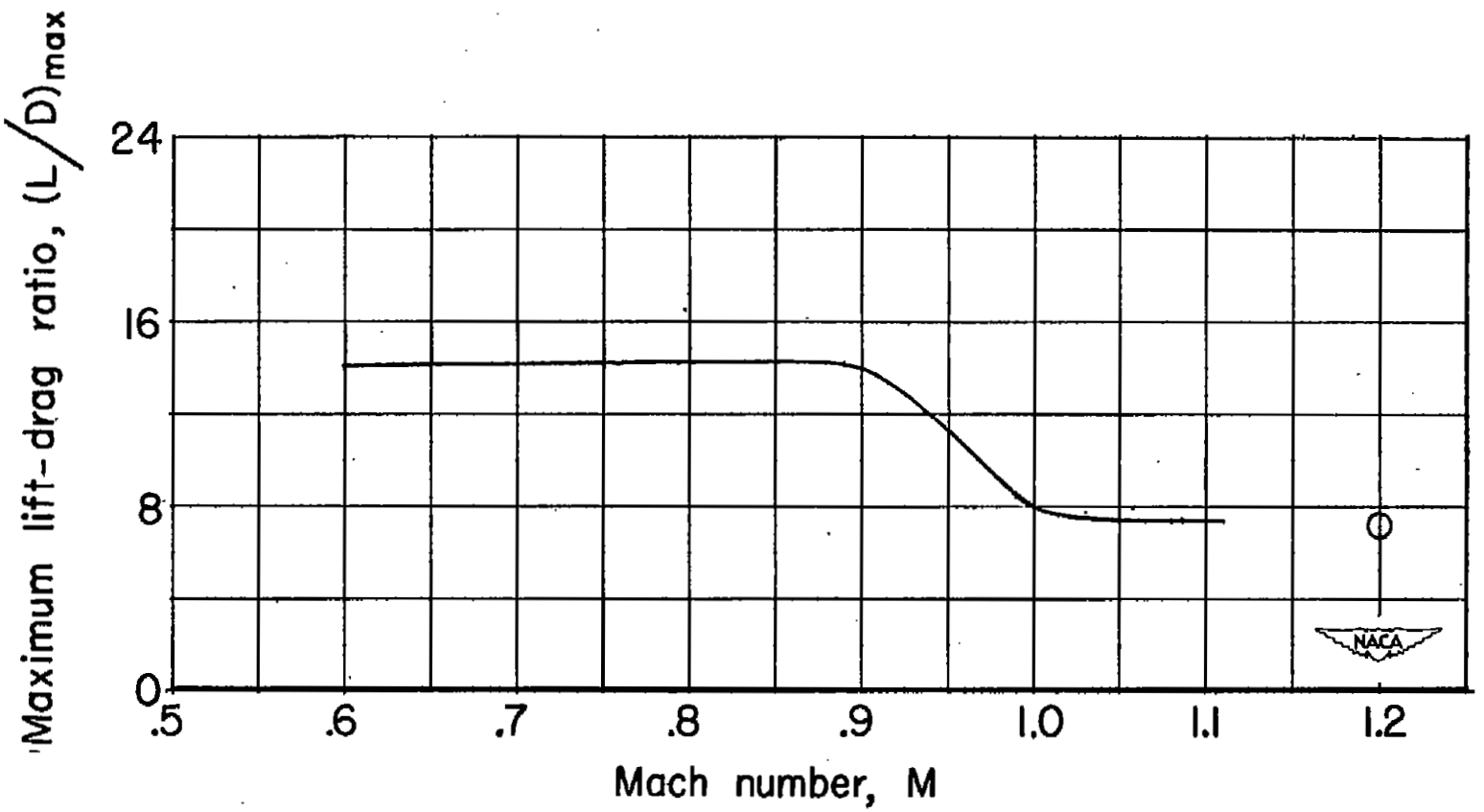

Figure 21.- Variation with Mach number of maximum lift-drag ratio for the wing-fuselage configuration. Drag corrected for sting interference. Data at M = 1.2 from reference 5.

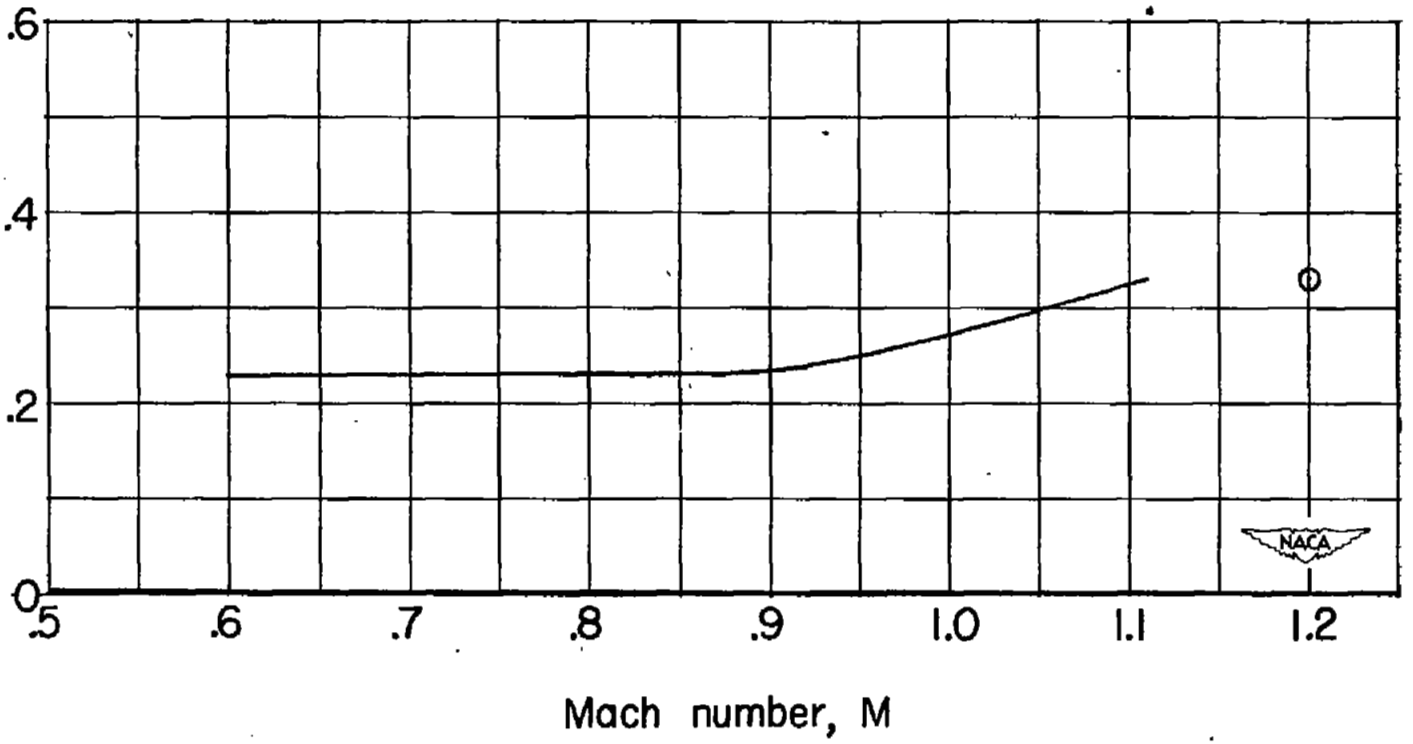

Figure 22.- Variation with Mach number of the lift coefficient for maximum lift-drag ratio for the wing-fuselage configuration. Drag corrected for sting interference. Data at M = 1.2 from reference 5.

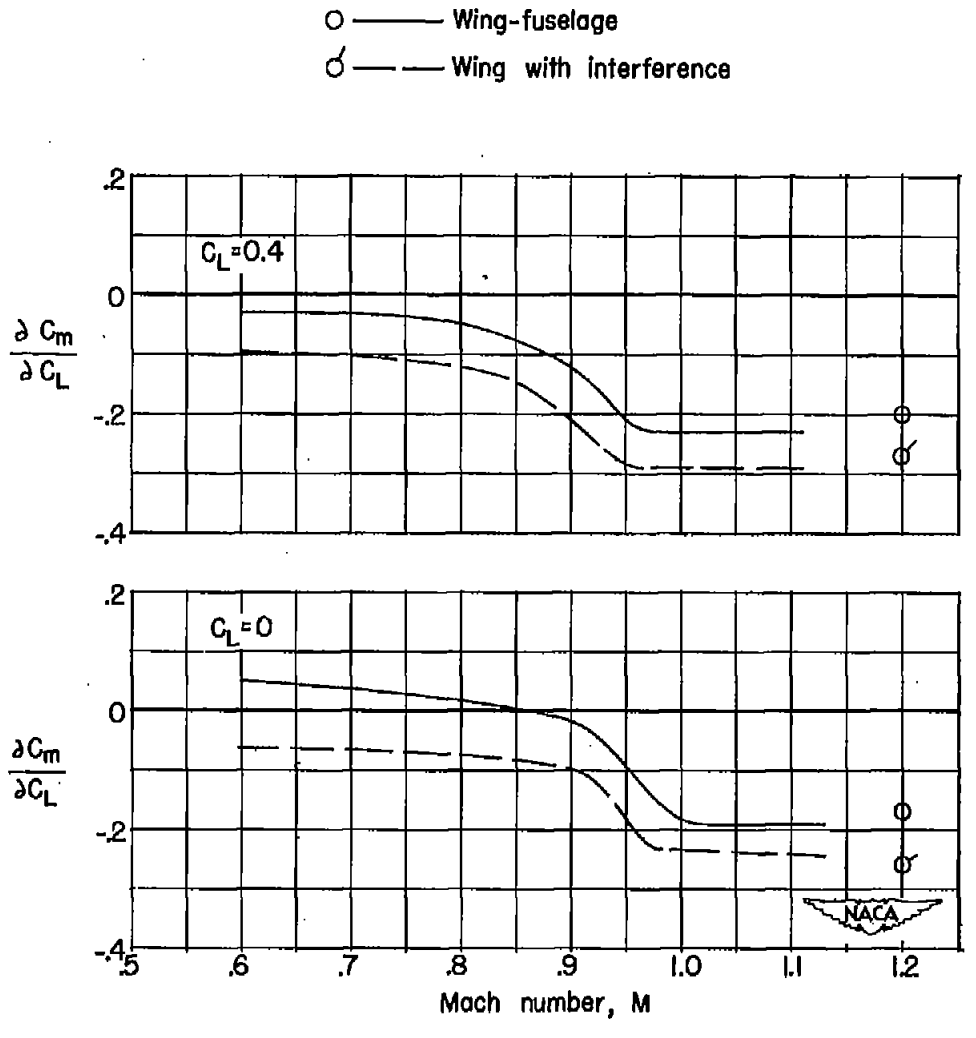

Figure 23.- Variation with Mach number of the static-longitudinal-stability parameter for the wing-fuselage configuration and for the wing with interference. Data at M = 1.2 from reference 5.

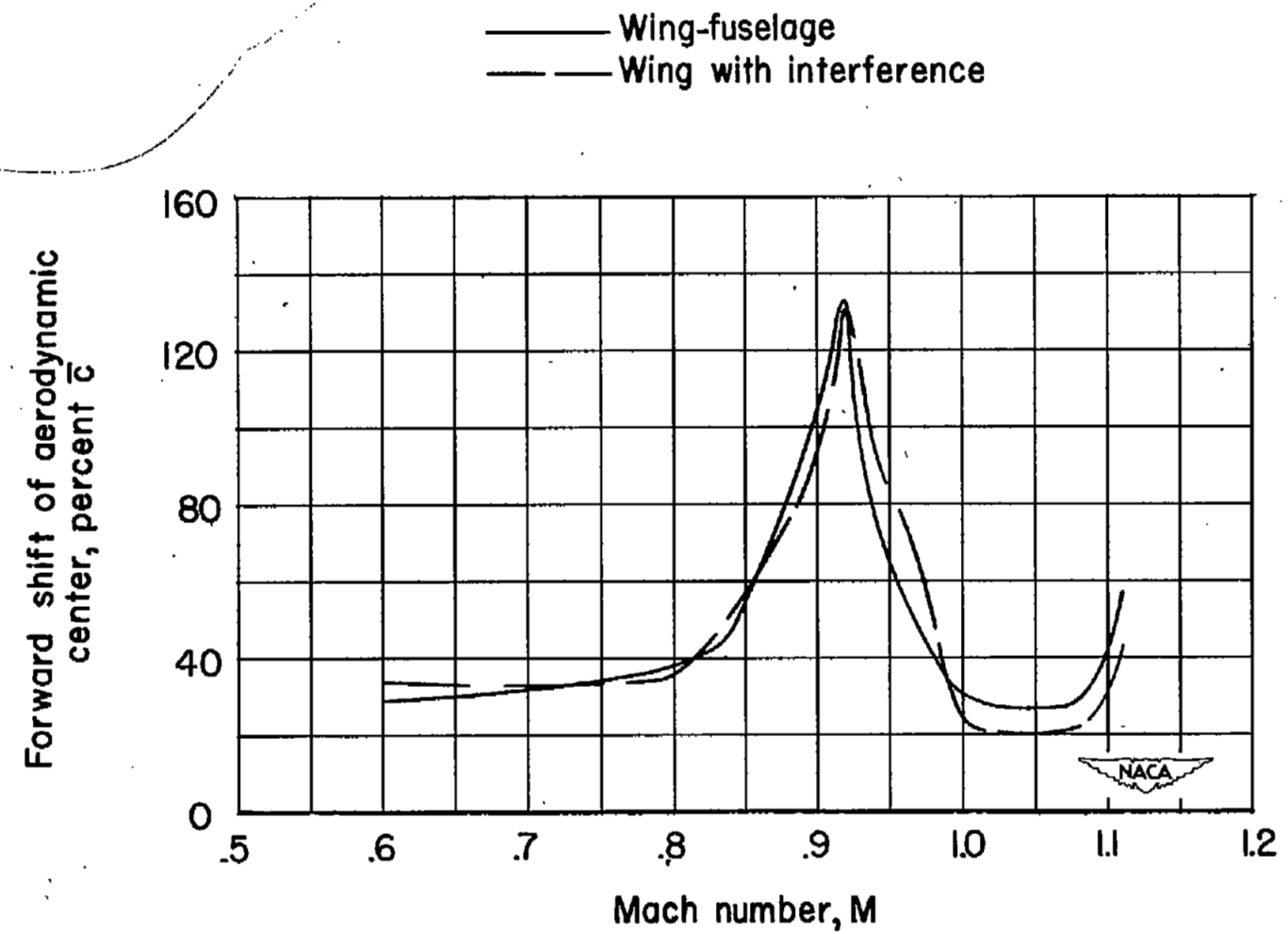

Figure 24.- Variation with Mach number of the forward shift in aerodynamic center in percent mean aerodynamic chord which occurred at moderate lift coefficients for the wing-fuselage configuration and for the wing with interference.

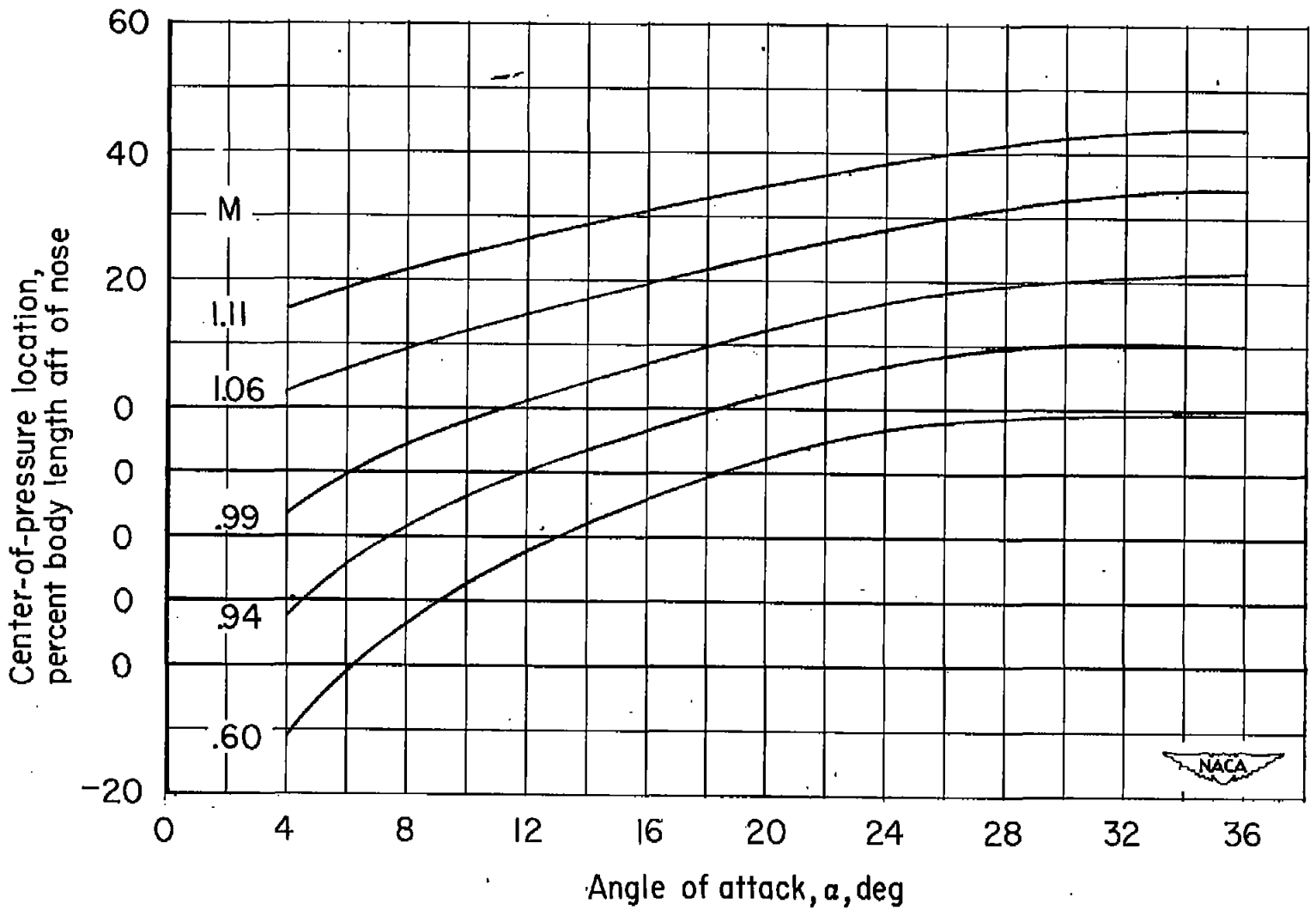

Figure 25.- Variation with angle of attack of center-of-pressure location for the original fuselage.

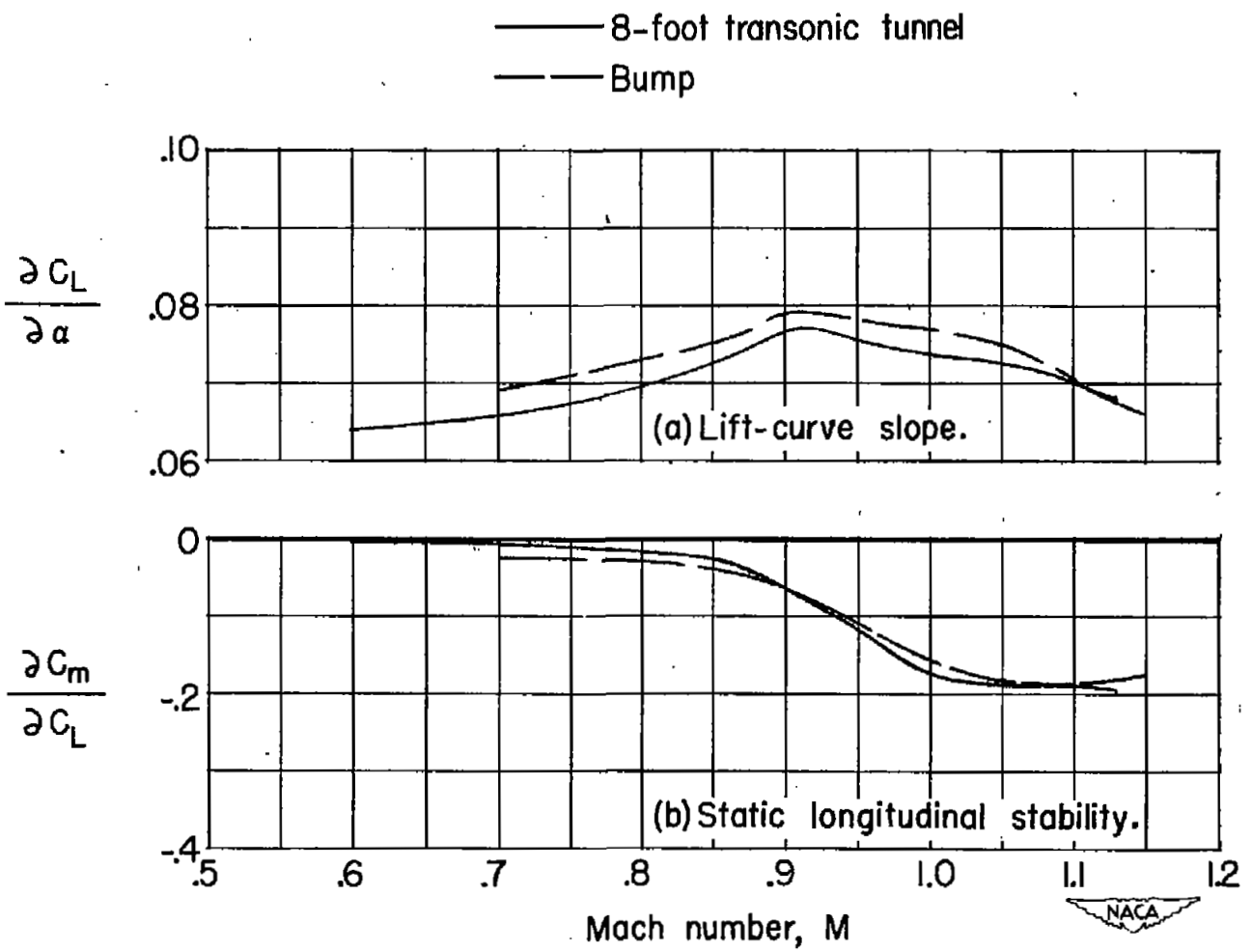

Figure 26.- Comparison of variation with Mach number of average lift-curve slope and static-longitudinal-stability parameter for the wing-fuselage configuration and for a similar model tested by the transonic-bump technique.

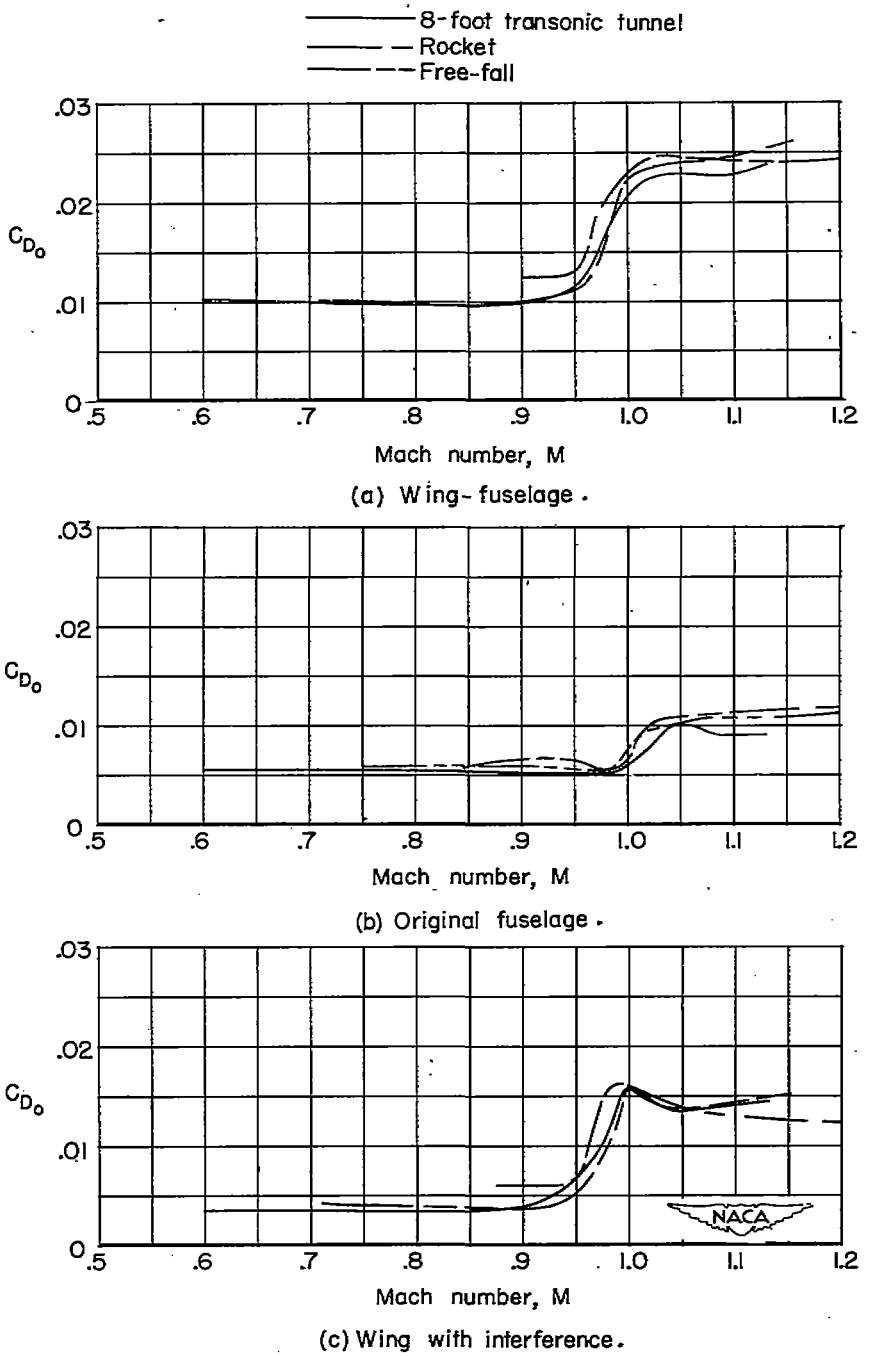

Figure 27.- Comparison of variation with Mach number of drag coefficient at zero lift for the wing-fuselage and original fuselage configurations and for the wing with interference as determined by different test techniques. Langley 8-foot transonic-tunnel data corrected for sting interference.

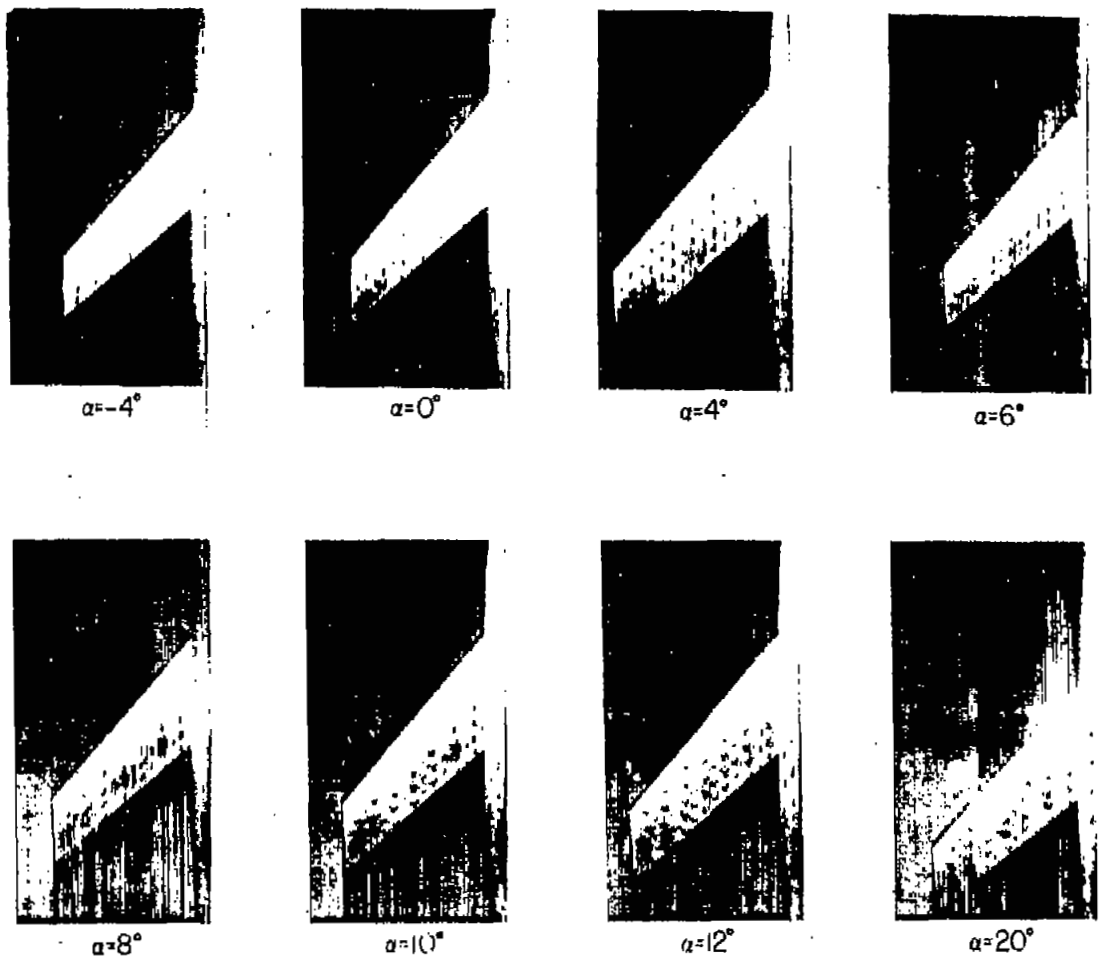

(b) M = 0.79.

Figure 28.- Continued.

NACA

I-75105

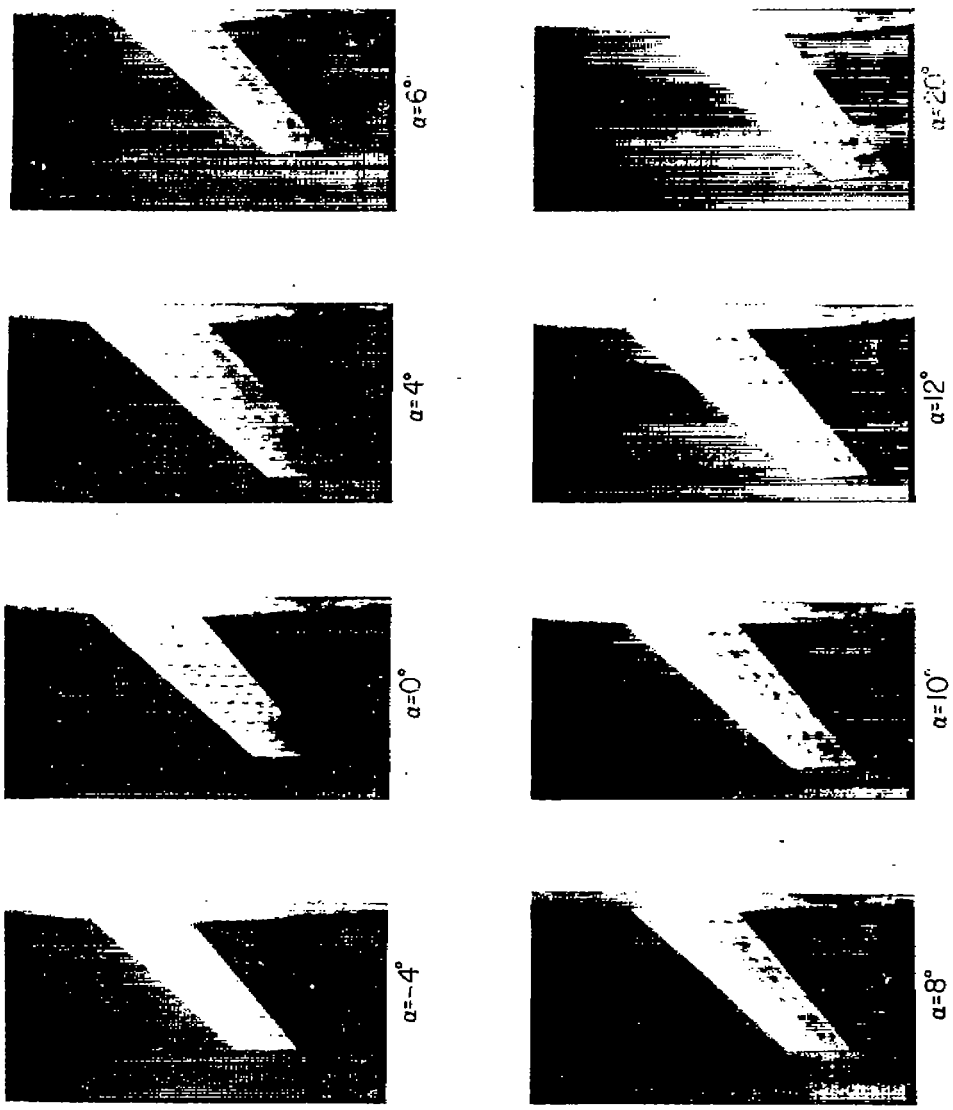

(c) M = 0.84. L-75106

Figure 28.- Continued.

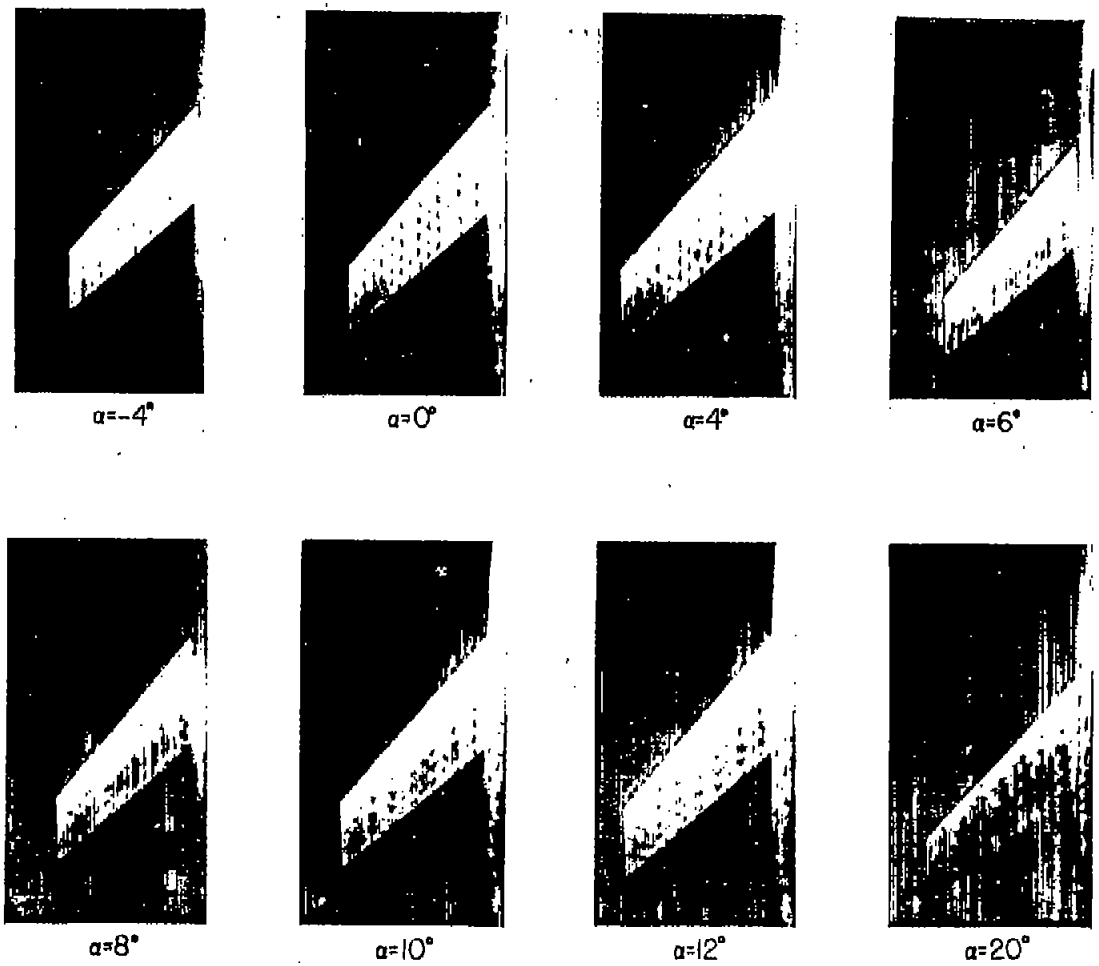

(d) M = 0.89.

NACA

I-75107

Figure 28.- Continued.

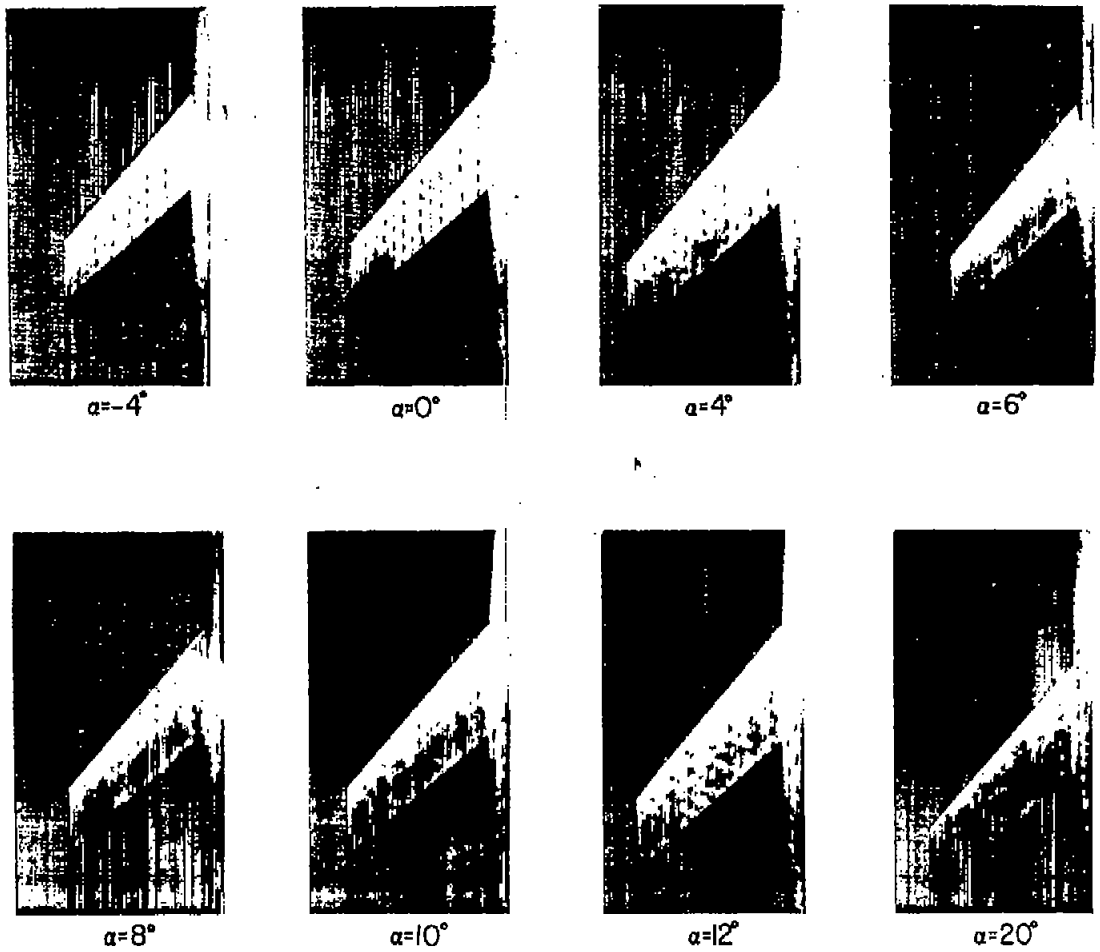

(e) M = 0.94.

I-75108

Figure 28.- Continued.

(f) M = 0.99.

NACA L-75109

Figure 28.- Continued.

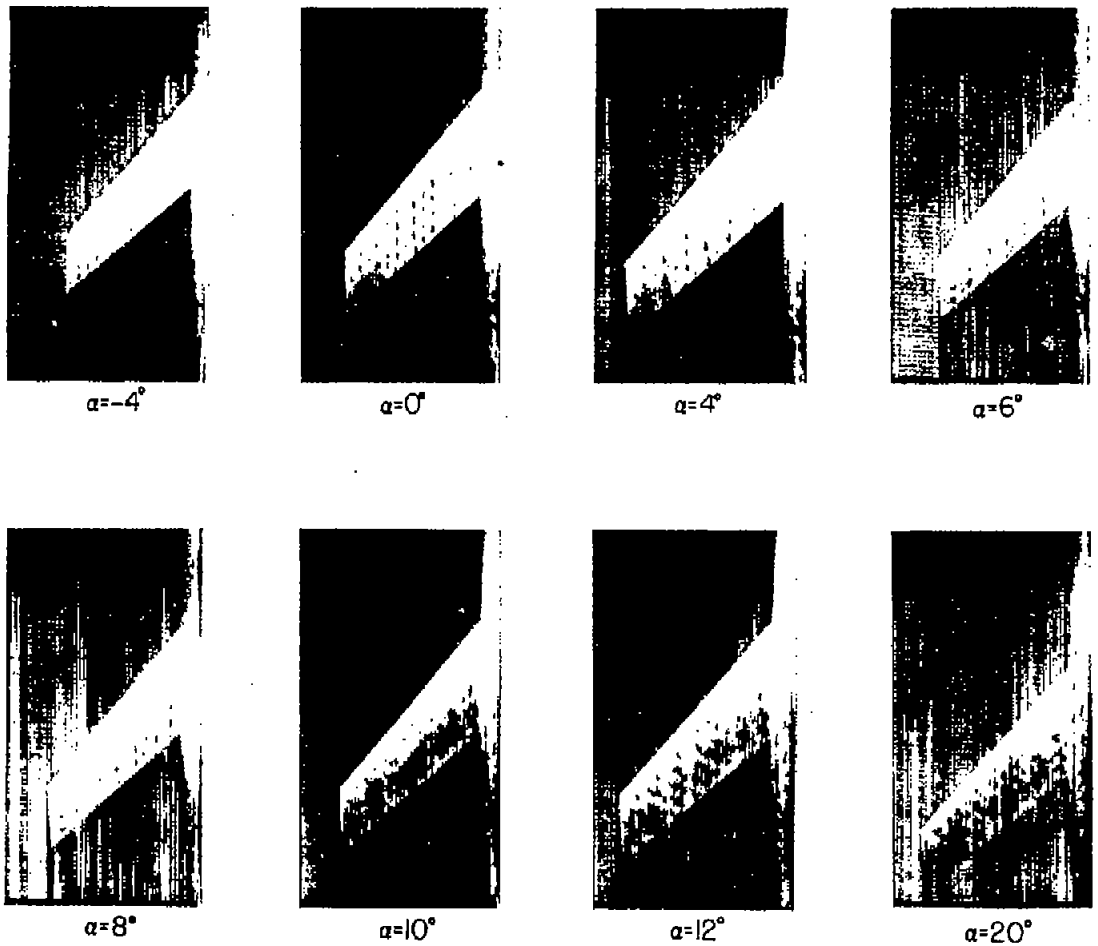

(g) M = 1.01.

NACA L-75110

Figure 28.- Continued.

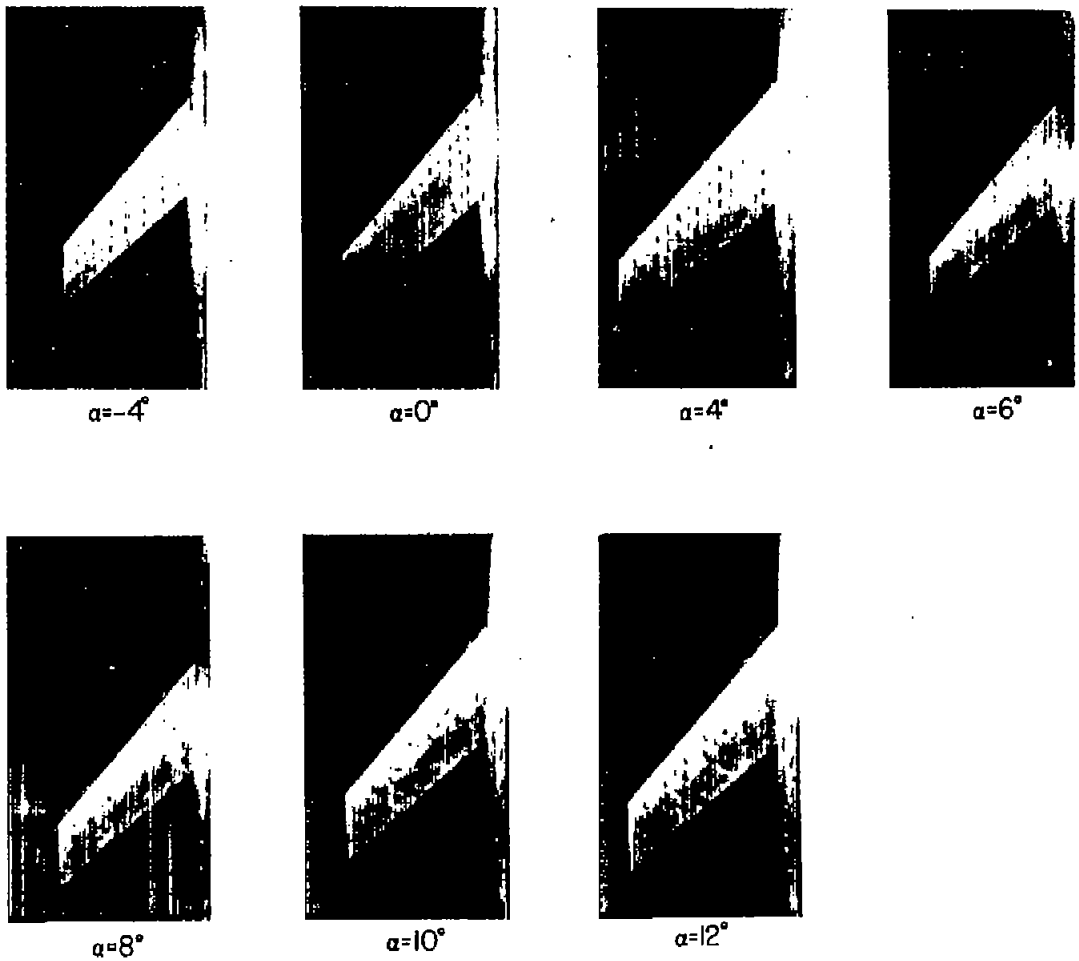

(i) M = 1.11.

L-75112

Figure 28.- Concluded.

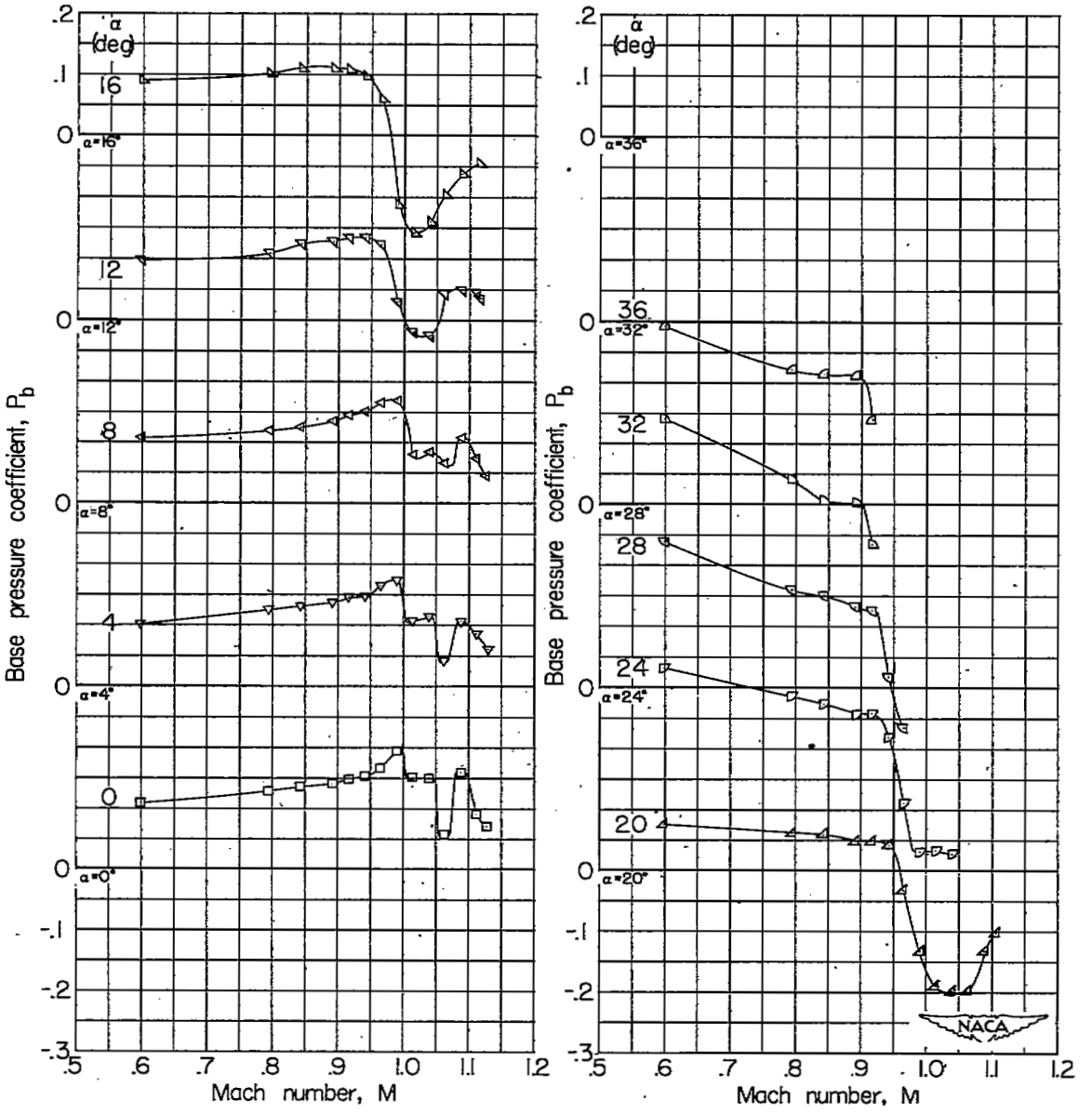

Figure 29.- Variation with Mach number of the base pressure coefficient for the wing-fuselage configuration.

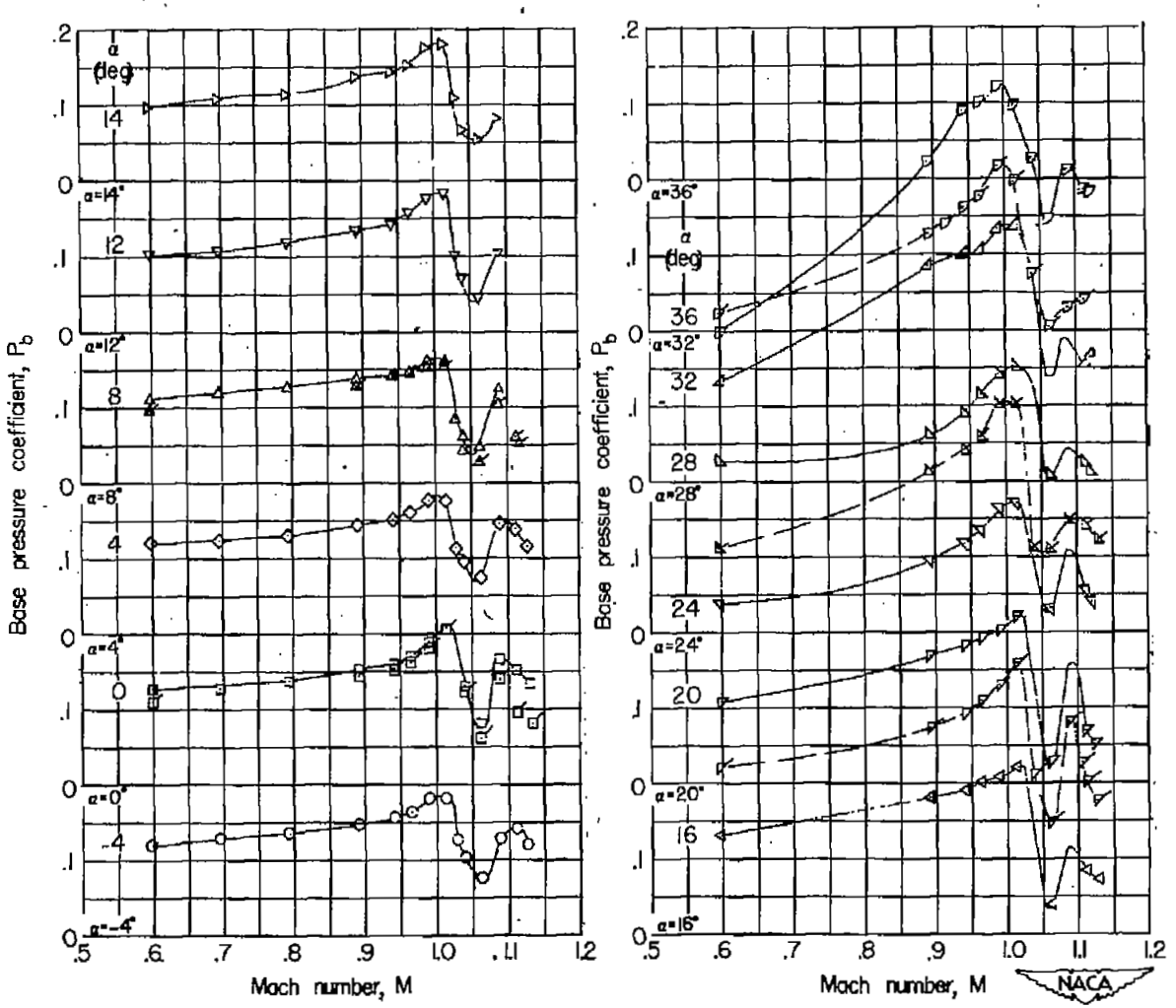

Figure 30.- Variation with Mach number of the base pressure coefficient for the original fuselage and fuselage configurations. Flagged symbols denote data for the fuselage configuration.

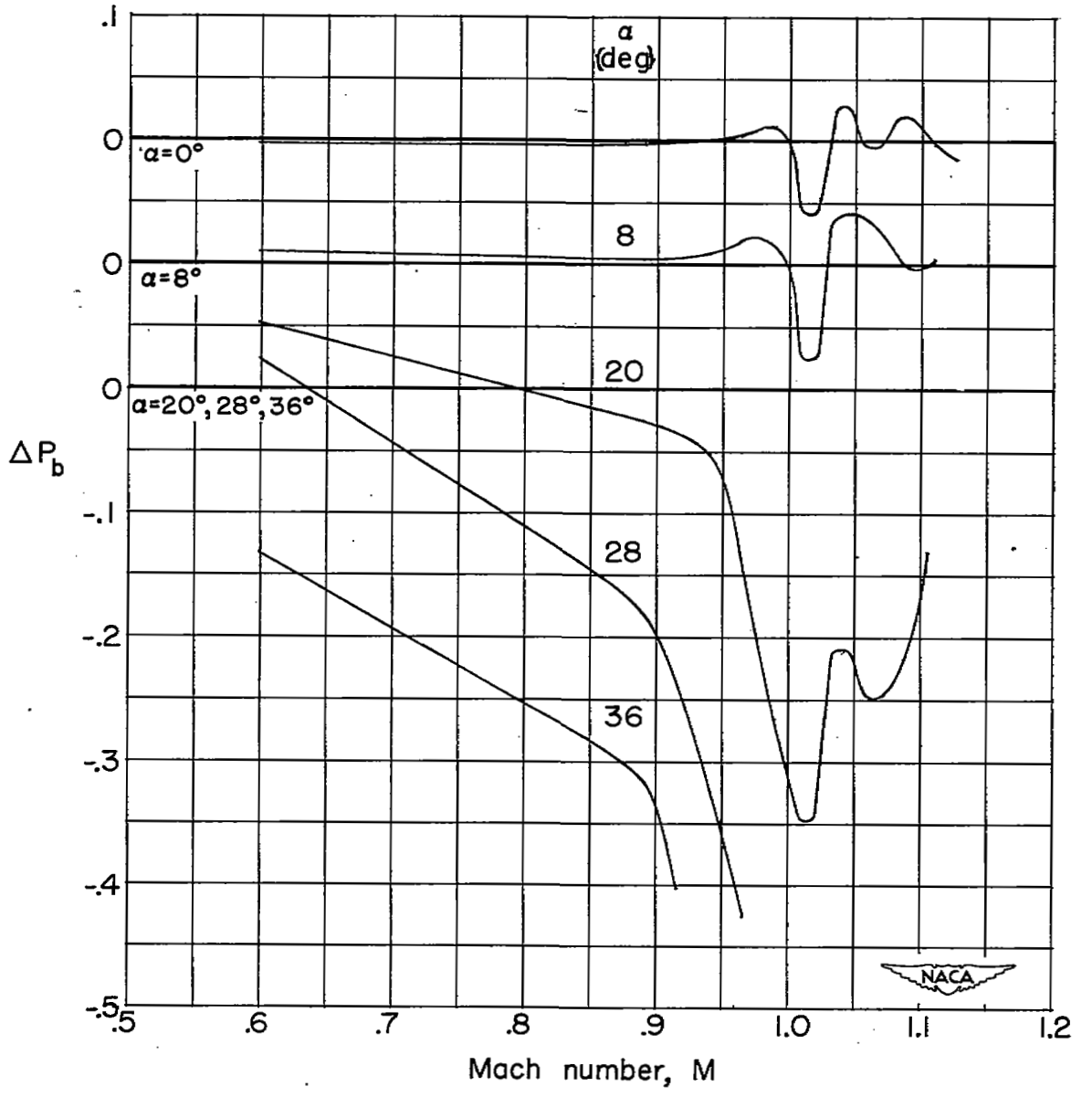

Figure 31.- Variation with Mach number of the incremental base pressure coefficient due to the addition of the wing to the fuselage.

NACA-Langley - 9-16-52 - 350

SECURITY INFORMATION

[redacted]

[redacted]